Icarus 258 (2015) 267–288

Contents lists available at ScienceDirect

Icarus

journal homepage: www.elsevier.com/locate/icarus

Impact and cratering rates onto Pluto

Sarah Greenstreet [a,*], Brett Gladman [a], William B. McKinnon [b]

[a] Department of Physics & Astronomy, 6224 Agricultural Road, University of British Columbia, Vancouver, British Columbia, Canada
[b] Department of Earth and Planetary Sciences and McDonnell Center for the Space Sciences, One Brookings Drive, Washington University, St. Louis, MO 63130, United States

ARTICLE INFO

Article history:
Received 12 December 2014
Revised 22 May 2015
Accepted 27 May 2015
Available online 4 June 2015

Keywords:
Pluto
Charon
Cratering
Kuiper belt

ABSTRACT

The New Horizons spacecraft fly-through of the Pluto system in July 2015 will provide humanity's first data for the crater populations on Pluto and its binary companion, Charon. In principle, these surfaces could be dated in an absolute sense, using the observed surface crater density (# craters/km^2 larger than some threshold crater diameter D). Success, however, requires an understanding of both the cratering physics and absolute impactor flux. The Canada-France Ecliptic Plane Survey (CFEPS) L7 synthetic model of classical and resonant Kuiper belt populations (Petit, J.M. et al. [2011]. Astron. J. 142, 131–155; Gladman, B. et al. [2012]. Astron. J. 144, 23–47) and the scattering object model of Kaib et al. (Kaib, N., Roškar, R., Quinn, T. [2011]. Icarus 215, 491–507) calibrated by Shankman et al. (Shankman, C. et al. [2013]. Astrophys. J. 764, L2–L5) provide such impact fluxes and thus current primary cratering rates for each dynamical sub-population. We find that four sub-populations (the $q < 42$ AU hot and stirred main classicals, the classical outers, and the plutinos) dominate Pluto's impact flux, each providing ≈ 15—25% of the total rate. Due to the uncertainty in how the well-characterized size distribution for Kuiper belt objects (with impactor diameter $d > 100$ km) connects to smaller projectiles, we compute cratering rates using five model impactor size distributions: a single power-law, a power-law with a knee, a power-law with a divot, as well as the "wavy" size distributions described in Minton et al. (Minton, D.A. et al. [2012]. Asteroids Comets Meteors Conf. 1667, 6348) and Schlichting et al. (Schlichting, H.E., Fuentes, C.I., Trilling, D.E. [2013]. Astron. J. 146, 36–42). We find that there is only a small chance that Pluto has been hit in the past 4 Gyr by even one impactor with a diameter larger than the known break in the projectile size distribution ($d \approx 100$ km) which would create a basin on Pluto ($D \geqslant 400$ km in diameter). We show that due to present uncertainties in the impactor size distribution between $d = 1$—100 km, computing absolute ages for the surface of Pluto is entirely dependent on the extrapolation to small sizes and thus fraught with uncertainty. We show, however, what the ages would be for several cases and illustrate the relative importance of each Kuiper belt sub-population to the cratering rate, both now and integrated into the past. In addition, we compute the largest "fresh" crater expected to have formed in 1 Gyr on the surface of Pluto and in 3 Gyr on Charon (to 95% confidence) and use the "wavy" size distribution models to predict whether these largest "fresh" craters will provide surfaces for which portions of the crater production function can be measured should most of the target's surface appear saturated. The fly-through results coupled with telescopic surveys that bridge current uncertainties in the $d = 10$—100 km regime should eventually result in the population estimate uncertainties for the Kuiper belt sub-populations, and thus the impact fluxes onto Pluto and Charon, dipping to $< 30\%$. We also compute "disruption timescales" (to a factor of three accuracy) for Pluto's smaller satellites: Styx, Nix, Kerberos, and Hydra. We find that none of the four satellites have likely undergone a catastrophic disruption and reassembly event in the past ≈ 4 Gyr. In addition, we find that for a knee size distribution with $\alpha_{faint} \leqslant 0.4$ (down to sub-km diameters), satellites of all sizes are able to survive catastrophic disruption over the past 4 Gyr.

1. Introduction

The New Horizons space probe will fly through the Pluto system in July 2015 and will be capable of taking high-resolution images of craters down to $\simeq 0.5$ km in diameter on the encounter hemispheres of Pluto and Charon (Young et al., 2008; Moore et al., 2014)[1]. Using the observed surface crater densities, one would like to compute crater retention ages for the various surfaces of

[1] Now that the final fly-by geometry has been determined, the resolution of the craters on the four smaller satellites has been calculated to be down to $\simeq 0.5$ km in diameter on Nix, down to $\simeq 1$ km on Hydra, and $\simeq 3$ km on Styx and Kerberos.

* Corresponding author.

http://dx.doi.org/10.1016/j.icarus.2015.05.026
0019-1035/

Pluto, its binary companion Charon, and the small satellites. In order to do this, knowledge of the impact flux onto the surface is needed, both in terms of the number of projectiles and their impact speeds. To date, a study of the impact rates broken down into the various Kuiper belt sub-populations has never been done. Lacking any crater data, particle-in-a-box methods or approximations of the number density of Kuiper belt objects that intersect the orbit of Pluto at an average impact velocity have sufficed (Weissman and Stern, 1994; Durda and Stern, 2000; Zahnle et al., 2003), but the observational opportunity of the New Horizons Pluto-system fly-through requires a more accurate understanding of the impact rates, impact speed distributions, and thus the collisional history of the surface of Pluto and its satellites.

1.1. Motivation

Pluto likely formed in a different environment from the one in which it currently resides. Some recent dynamical models postulate a violent period of instability in the giant planet orbits roughly 3.9 Gyr ago (Hahn and Malhotra, 1999; Gomes, 2003; Tsiganis et al., 2005); during this chaotic time period, an outward migration of Uranus and Neptune causes their orbits to approach each other, briefly pumping Neptune's eccentricity which pushes the ancient population of Kuiper belt objects outward and rearranges the outer Solar System to roughly its current architecture (Levison et al., 2008 and references therein). With or without a dramatic planetary re-arrangement 3.9 Gyr ago, in any scenario in which Neptune's mean-motion resonances swept through a population of small bodies during outward migration, many objects, including Pluto, are swept up into resonance (Malhotra, 1993, 1995). Regardless of exactly how it arrived there, Pluto currently sits in the 3:2 mean-motion resonance with Neptune. A hypothetical turbulent time period during the first $\approx$ 500 Myr of Solar System history we refer to as the "pre-installation phase" of Pluto's collisional history, and is not something we can model using estimates of today's Kuiper belt orbital distribution. We assume the Pluto–Charon binary-forming event occurred during this "pre-installation phase". Because we do not know the orbital distribution of the Kuiper belt during this period of the Solar System's history, we prefer to remain on relatively solid ground by performing an analysis of Pluto's collisional history for the past $\simeq$ 3.9 Gyr, spanning the time period we think it reasonably certain Pluto has been on its current orbit, $t \approx 0.6$ Gyr to 4.5 Gyr into the age of the Solar System. We refer to this period as the "post-installation phase" of Pluto's history. Pluto's current location in the Kuiper belt causes it to be impacted by a wider variety of Kuiper belt sub-populations than the satellites of the giant planets, particularly by the cold classical objects, which do not reach into the giant planet region. We use current population estimates and orbital distributions of Kuiper belt sub-populations to determine the current impact flux and primary cratering rates onto the surface of Pluto in Sections 2.3 and 2.4. To extrapolate this back to the installation of Pluto onto its current orbit (not less than 3.9 Gyr ago), we assume each Kuiper belt sub-population has naturally decayed away with time and we use estimates of these decay rates from the literature to compute the number of primary craters formed on Pluto's surface integrated over the past $\simeq$ 4 Gyr in Section 2.5 (secondary craters are considered separately in Section 3.5). We also compute the primary cratering rates and integrated number of craters for the surface of Charon in Section 3.7. In addition, we determine if the four smaller satellites of Pluto (Styx, Nix, Kerberos, and Hydra) have likely ever been catastrophically disrupted in the past $\simeq$ 4 Gyr in Section 3.8.

1.1.1. Kuiper belt sub-populations

As defined in Gladman et al. (2008), the various Kuiper belt sub-populations are divided as follows. Resonant objects are those currently in a mean-motion resonance with Neptune. Scattering objects are those which over 10 Myr integrations experience encounters with Neptune resulting in a semimajor axis a deviation of more than 1.5 AU.[2] Classical or detached bodies are further sub-divided into the inner classical objects (a interior to the 3:2 mean-motion resonance), main classical objects (a between the 3:2 and 2:1 mean-motion resonances), outer classical objects (a exterior to the 2:1 mean-motion resonance and eccentricity $e < 0.24$), and the detached objects (a beyond the 2:1 mean-motion resonance with $e > 0.24$). For our work, the detached objects and outer classical objects are combined, as both have semimajor axes greater than Pluto's aphelion ($a > Q_{Pluto}$).

We further subdivide the classical main belt into hot (wide inclination distribution) and cold (narrow inclination) components, where the cold population contains stirred and kernel sub-components, as defined in (Petit et al., 2011). The hot classical main objects have $a = 40$—47 AU, perihelia $q = 35$—40 AU, and an inclination distribution proportional to $\sin(i)$ times a Gaussian with a width of 16°. The stirred cold classical objects have $a = 42.4$—47 AU, a q distribution that is a function of semimajor axis (Petit et al., 2011), and an inclination distribution proportional to $\sin(i)$ times a Gaussian with a width of 2.6°. Lastly, the kernel cold classical objects have $a = 43.8$—44.4 AU, $e = 0.03$—0.08, and the same inclination distribution as the stirred cold classical objects.

It was unclear at the outset of this project how the various Kuiper belt sub-populations would contribute to the impact flux onto the surface of Pluto. Each group populates different regions of phase space and thus interacts differently with Pluto, but how their respective impact fluxes compare with each other is not obvious. In previous work (e.g. Zahnle et al. (2003)), a Kuiper belt having objects with "typical" semimajor axes $a \approx 40$ AU and "typical" impact speeds $v_{impact} \approx 2$ km/s was used to roughly estimate the cratering rate onto Pluto. This, however, neglects the details of the differing orbital parameters of each Kuiper belt sub-population. It's unclear whether Kuiper belt objects (KBOs) with these estimated orbital parameters contribute most of the impact flux onto Pluto or another type of Kuiper belt population dominates. Perhaps several populations contribute roughly equally. Campo Bagatin and Benavidez (2012) computed the collision probability of the Pluto–Charon binary-forming event using a collisional evolution model of the transneptunian object (TNO) population taken from the Canada-France Ecliptic Plane Survey (CFEPS) L7 synthetic model of classical and resonant Kuiper belt populations (Petit et al., 2011; Gladman et al., 2012), but did not break this down into the individual Kuiper-belt sub-populations nor extend their analysis to the current epoch's impact events.

Pluto shares the 3:2 neptunian mean-motion resonance with $\approx 13,000$ diameter $d > 100$ km (Gladman et al., 2012) objects known as the plutinos. By performing numerical integrations of the collisional evolution of known plutinos, de Elía et al. (2010) computed the plutino impact flux onto Pluto assuming "typical" impact speeds ($v_{impact} = 1.9$ km/s) to estimate the cratering rate onto Pluto from the plutinos alone. Dell'Oro et al. (2013) performed a statistical analysis of the collisional evolution of TNOs among themselves using the individual Kuiper belt sub-populations from the CFEPS L7 model, but did not extend their analysis to the cratering rate on Pluto. As we were writing up our work, we became aware of the recent paper by Bierhaus and Dones (2015) that

[2] The reader is cautioned that in the literature, the term "scattered disk" often refers to objects which have either scattered off Neptune in the past and are now decoupled from Neptune (but have perihelia near Neptune's aphelion at $q \approx 30$ AU; i.e., what we define to be the detached objects) or are actively scattering off Neptune currently (i.e., what we define to be the scattering objects (Gladman et al., 2008)). The detached objects are also sometimes referred to as the "extended scattered disk" in the literature (Gladman et al., 2008).

addresses some of the issues we are concerned with. We discuss this latter paper in Section 2.3.

In addition to being affected by the 3:2 mean-motion resonance with Neptune, Pluto's orbit experiences Kozai (Kozai, 1962) librations which cause its eccentricity e and inclination i to oscillate against each other (high-e corresponds to low-i and vice versa) on the timescale of several Myr. This libration causes Pluto's orbit[3] to never intersect the Solar System plane outside $\simeq 42$ AU or inside $\simeq 33$ AU (see Fig. 1). Fig. 1 shows Pluto's ecliptic nodal distance behavior over a 6 Myr time period, but it is believed this behavior has been occurring during the entirety of Pluto's "post-installation" period over the past 4 Gyr. This results in complex changes in collision probability over time between Pluto and the inner, main, and outer classical Kuiper belt objects. For example, the classical inner KBOs have a between roughly 37 and 39 AU with perihelia 35 AU $\lesssim q \lesssim$ 39 AU. This places the classical inner KBOs in the region where Kozai librations keep Pluto's ecliptic nodal distances. As one may imagine, Pluto's nodal distances constantly staying near the classical inner KBOs enhances their collision probability with Pluto compared with a situation where Pluto's orbit uniformly precesses and nodal distance explores all values from perihelion q_{Pluto} to aphelion Q_{Pluto}. In contrast, most main classical KBOs lie between roughly 40 and 47 AU where the oscillation of Pluto's ecliptic nodal distances cause its periodic intersection with the main classical KBOs. If all classical main KBOs had inclinations $i \approx 0°$, the $q > 42$ AU classical main objects should have zero collision probability with Pluto since Pluto's orbit never intersects the plane of the Solar System outside $\simeq 42$ AU. In reality, their non-zero inclinations cause some of them to have non-zero collision probability with Pluto. The two $q < 42$ AU classical main populations (and their sub-components), however, are each affected by the repeated intersection of Pluto's orbit with its own. During the period when Pluto's nodal distance is between 40 and 42 AU, its collision probability with the main classical KBOs increases. This competes with the times when Pluto's orbit intersects the plane of the Solar System outside 42 AU, where its collision probability with the main classical Kuiper belt drops precipitously. As one may expect, this could cause the $q < 42$ AU classical main KBOs to receive a smaller enhancement to their collisional probability with Pluto than the classical inner KBOs since the assumption of uniform orbital precession would also cause an orbital intersection oscillation. Lastly, the classical outer KBOs also experience complex changes in collision probability with Pluto over time. The classical outer KBOs, which in this study include the detached objects, have pericenters between $\simeq 33$ AU and $\simeq 42$ AU, the same region where Pluto's nodal distances remain. However, the classical outer KBOs have semimajor axes from roughly 47 AU out to $\simeq 500$ AU causing them to only impact Pluto when they are near pericenter, dropping their collision probability. How do each of these competing phenomena affect the impact flux onto Pluto from the classical KBO sub-populations? Likewise, how do each of the complex interactions between Pluto and the Kuiper belt sub-populations stack up against each other when determining Pluto's cratering history? The answers are not obvious and provided some of the motivation for this study.

An additional complexity is that gravitational scattering has depleted each sub-population over the past 3.9 Gyr, but affecting each population differently. How this population decay affects the impact flux at Pluto when integrated over the age of the Solar System is also unclear. For example, the scattering objects spend a large fraction of their time at large distances from Pluto making their collisional cross-section with Pluto small. However, they are also thought to be one of the largest populations in the Kuiper belt 4 Gyr ago (Duncan and Levison, 1997; Levison and Duncan, 1997; Dones et al., 2004), which increases their contribution to Pluto's cratering history when integrated over the age of the Solar System. This large population decay competes with the low collisional cross-section of the scattering objects when determining their contribution to the cratering history of Pluto, but is the large number of scattering objects in the past enough to dominate the cratering rate over other Kuiper belt sub-populations? To best understand the contribution of each Kuiper belt sub-population to the cratering history of Pluto, a study using the impact flux of debiased population models and their corresponding impact speed distributions is needed and presented here.

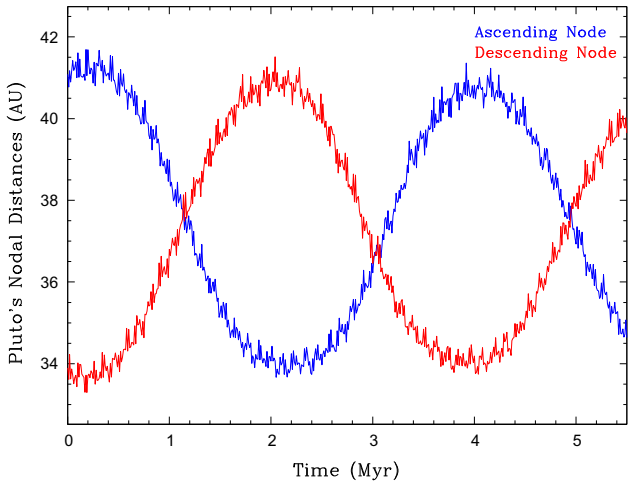

Fig. 1. Numerical integration of Pluto's ecliptic nodal distances.

1.1.2. Uncertainties in the Kuiper belt size distribution

In addition to the dynamical complexities of the Pluto-crossing populations, there are major uncertainties about the Kuiper belt size distribution for objects with absolute g-band magnitude $H_g > 9.16$ (corresponding to a diameter $d < 100$ km for an assumed g-band albedo p of 5% using the following)

$$d \backsimeq 100 \text{ km} \sqrt{\frac{0.05}{p}}\, 10^{0.2(9.16-H_g)} \tag{1}$$

Eq. (2) defines the differential number of objects N as a function of H-magnitude, where α is the logarithmic "slope" (hereafter referred to simply as the slope) and allows mapping to the differential distribution in diameter d given in Eq. (3) by $q_{slope} = 5\alpha + 1$.

$$dN \propto 10^{(\alpha * H)} \tag{2}$$

$$dN \propto d^{(-q_{slope})} \tag{3}$$

The Kuiper belt impactor size distribution has recently been absolutely calibrated down to $H_g \approx 8$–9 by the CFEPS survey (Petit et al., 2011; Gladman et al., 2012). The $H_g = 4$–9 range seems well modeled by a single slope α in a given population, where the only caveat to this would be the hot and cold components of the main classical Kuiper belt population which appear to have different values of α (Bernstein et al., 2004, 2006; Petit et al., 2011; Fraser et al., 2014; Adams et al., 2014). It is clear that a single power law extended past $H_g = 9$ does not fit the observations, and that some kind of a break in the differential size distribution at this H_g-magnitude is a better representation (Jewitt et al., 1998; Gladman et al., 2001; Bernstein et al., 2004; Fraser and Kavelaars, 2008; Fuentes and Holman, 2008; Shankman et al., 2013; Fraser et al., 2014; Adams et al., 2014). Because we wish to estimate crater production rates down to km scale, we must adopt a model of how the size

[3] For reference Pluto's perihelion $q = 29.7$ AU and aphelion $Q = 48.9$ AU.

distribution extrapolates from the break at $d \simeq 100$ km down to sub-km impactor sizes. We adopt a break at $H_g \approx 9$ (for typical TNO $g-r$ colors of 0.5–1.0, the break at $H_g \sim 9$ is shifted to $H_r \sim 8$–8.5, which is consistent with Fraser et al.'s (2014) results for the hot KBO and jovian trojan populations). Fig. 2 shows a schematic of three size distribution extrapolation scenarios for $H_g > 9$. The (somewhat strawman) single power-law (SPL) extends the bright end of the size distribution ($H_g < 9$) all the way down to the smallest objects. The model size distribution with a "knee" has a sharp break at $H_g = 9$ (open circle) from a steep slope at the bright end of this H_g-magnitude to a shallower slope on the faint end. Lastly, the "divot" model has a discontinuous drop by a factor c in the differential number of objects at $H_g = 9$ with a different power law for $H_g > 9$. All of these models are of course approximations to reality; we discuss the implications of changing α_{faint} and using a "wavy" size distribution in Sections 3.4 and 3.6, respectively.

To illustrate the consequences of not understanding how the relatively well-understood size distribution of large impactors connects to smaller sizes, we model five differential size distribution scenarios: a single power-law (SPL) with logarithmic slope $\alpha = 0.8$ ($q_{bright} = 5$); a power-law with a sharp knee at $H_g = 9.0$, slope $\alpha_{bright} = 0.8$ on the bright side of the knee, and slope $\alpha_{faint} = 0.4$ ($q_{faint} = 3$) on the faint side of the knee; a power-law with a "divot" at $H_g = 9.0$ with the same α_{bright} and α_{faint} as the knee scenario, but with a contrast (ratio of the differential number of objects in the population just bright of the divot to the number of objects just faint of the divot) value of $c = 6$ (the least rejectable (with factors of several uncertainty) size distribution fit from Shankman et al. (2013)); and lastly the "wavy" size distributions of both Schlichting et al. (2013) and Minton et al. (2012) (as described by Schlichting et al. (2013)).

Values for α_{faint} vary between 0.2 and 0.6 across various outer Solar System small body populations (Larsen et al., 2001; Trujillo et al., 2001; Szabó et al., 2007; Solontoi et al., 2012; Schlichting et al., 2013) as well as the Kuiper belt size distribution literature (Jewitt et al., 1998; Gladman et al., 2001; Bernstein et al., 2004; Fraser and Kavelaars, 2008; Fuentes and Holman, 2008; Shankman et al., 2013; Adams et al., 2014) down to the observational limit of $H_g \approx 8$–10 for the various sub-populations. We adopt a value of $\alpha_{faint} = 0.4$ (Bernstein et al., 2004; Fraser et al., 2014) for this work and discuss the implications of changing this value in Section 3.4. Although we assume a constant power law slope of the H_g-magnitude distribution from $d = 100$ km down to smaller sizes ($H_g = 9$–25), it is very unlikely that in reality the faint size distribution follows a single power-law all the way down to sub-km impactor sizes. We use a single extrapolation for simplicity's sake and to illustrate many of the consequences of not understanding the impactor size distribution down to $d < 100$ km to the cratering record on Pluto, but we understand that the size distribution in this regime likely has multiple slope changes which we refer to as being "wavy". The main asteroid belt's size distribution (O'Brien and Sykes, 2011), the analysis of saturnian craters from Minton et al. (2012), and the model for the collision-generated population of KBOs today from Schlichting et al. (2013) all show that several slopes in the size distribution begin as one drops below roughly $d < 60$ km and continue to the sub-km regime. We discuss the implications of such a shape in the size distribution on Pluto's cratering record compared with a single-slope extrapolation in Section 3.6.

Because New Horizons should be able to observe craters down to 1–2 km in diameter on the encounter hemispheres[4] of Pluto and

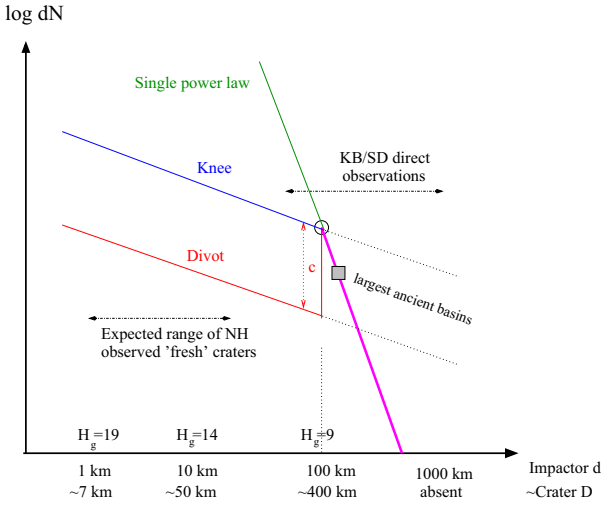

Fig. 2. Schematic of three H_g-magnitude differential size distribution scenarios: a single power-law (SPL) (green), a knee (blue), and a "divot" (red). The Kuiper belt and Scattering Disk observations are calibrated down to $H_g \approx 9$ (magenta), but beyond that (open circle) it is unclear how the size distribution extends to smaller sizes. The knee model is a simple transition to a shallower slope at the break diameter. The divot scenario has a rapid drop in the differential number of objects succeeded by a shallower recovery. H_g-magnitudes are converted to approximate impactor diameters d using Eq. (1) for an albedo p of 5%. Impactor diameters d are converted to rough crater diameters D using Eqs. (5), (6a), and (6b), assuming an impact speed of 2 km/s and a transition from simple to complex craters at 4 km on Pluto (Moore et al., 2014). The expected range of "fresh" craters observed by New Horizons extends from $D \approx 5$ km to $D \approx 50$ km (created by impactors ranging from $d = 1$–10 km), while the largest "ancient" basins ($D \approx 200$ km) are not expected to have been created in the past 4 Gyr and therefore must date to Pluto's pre-installation phase > 4 Gyr ago. (For interpretation of the references to color in this figure legend, the reader is referred to the web version of this article.)

Charon, and down to 500 m in diameter in a high-resolution swath (Young et al., 2008; Moore et al., 2014), the uncertainties in the form of the Kuiper belt's size distribution will be reflected in the computation of surface ages in the Pluto system. This is well into the small end of the size distribution (a $D = 500$ m crater corresponds to roughly a $d = 40$ m impactor), but the uncertainties in the Kuiper belt size distribution will be apparent in larger craters as well. For example, the number of impactors in the differential size distribution with diameter d near 10 km varies by a factor of 6 (the value of the contrast c) between the knee and divot scenarios and by a factor of 50 between the SPL and the knee distributions. Because the number of small impactors varies so widely between the three extrapolations, ages computed from observed crater densities based on these distributions naturally will rely heavily upon the intrinsic assumptions about the projectile size distribution. In addition, extrapolating the knee power-law size distribution from small diameters to projectiles just larger than the break (shown as dotted lines in Fig. 2) overestimates the number of "largest ancient basins expected", however, extrapolating the divot scenario underestimates the number of basins. Implications of these assumptions on both the computed crater retention ages (as opposed to the emplacement or crystallization age of a given surface unit, which may be older) and the determination of the impactor size distribution from Pluto's cratering record are discussed in Section 3.

1.1.3. Triton

Triton, Neptune's major moon, is the closest body to Pluto for which we have crater counts (from the 1989 Voyager 2 flyby). Triton's general characteristics (size, mass, and surface composition) are extremely Pluto-like. Triton is also a geologically active body, and thus lightly cratered, and so should record only recent impacts from the scattering KBO population. Leaving aside the

[4] Pluto–Charon's slow 6.39 day rotation combined with the speed of the New Horizons spacecraft mean that the non-encounter hemisphere will not be imaged at sufficient resolution and solar phase angle for meaningful crater counts.

debate over whether Triton's craters are predominantly due to heliocentric or planetocentric bodies (Schenk and Zahnle, 2007; McKinnon and Singer, 2010), the best global crater counts are from Schenk and Zahnle (2007). They find for *craters* between 5 and 25 km diameters (25 km being the size of the largest crater identified on the $\approx 25\%$ of the surface imaged decently by Voyager) a differential power-law index of 3.25. Using simple crater scaling, they calculate a differential q_{slope} of 2.8 ($\alpha = 0.36$) for the *projectile* population in the diameter range of $d = 300$ m to $d = 2$ km. Actually, because the craters span the simple-to-complex morphological transition, the actual q_{slope} and α are likely slightly steeper. In either case, such α values are close to the $\alpha = 0.4$ adopted here for the faint branch of the KBO distribution down to this diameter. This value of α is also not inconsistent with the Minton et al. (2012) and Schlichting et al. (2013) size distribution models for this impactor diameter range (see Section 3.6). It will be of great interest to see, in 2015 New Horizons images, if the crater size–frequency distributions on Pluto and Charon are similar to Triton's over comparable *projectile* diameter ranges.

2. Methods

In this section we present the methods used to compute current impact rates (Section 2.3), current cratering rates (Section 2.4), and the integrated number of craters on Pluto's surface over the past $\simeq 3.9$ Gyr (Section 2.5) from the various Kuiper belt sub-populations.

2.1. Kuiper belt population models

In order to most accurately determine Pluto's cratering history from the current Kuiper belt, we make use of the recent observational data encompassing each of the sub-populations. The Canada-France Ecliptic Plane Survey (CFEPS) L7 synthetic model (Petit et al., 2011; Gladman et al., 2012) was used to provide orbital distributions and $H_g < 9.16$ (diameter $d > 100$ km) population estimates for the resonant and classical Kuiper belt objects. However, the observed number of scattering objects provided a CFEPS orbital distribution that only samples the closest objects that need to then be extrapolated to larger distances. In contrast, the Kaib et al. (2011) (KRQ11) model provided a much more accurate representation of the scattering population as it evolves from the Oort Cloud; it is thus the current model of choice in this study for the orbital distribution of the scattering objects and was coupled to CFEPS to produce the absolutely-calibrated $H_g < 9.0$ population estimates of the scattering population by Shankman et al. (2013). Estimates from the Deep Ecliptic Survey (Adams et al., 2014) for some sub-populations were discrepant from the CFEPS estimates (Petit et al., 2011; Gladman et al., 2012) by factors of 1.5–1.7, but the surveys were acquired in different bandpasses; compiling the *g*-VR colors of objects seen in both surveys (K. Volk, private communication, 2015) showed that colors of 0.4–0.6 (rather than 0.1) were appropriate and this eliminates virtually all discrepancy in the *H*-magnitude range common to both surveys when using the same dynamical-class definitions.

In order to pin the number of objects in each of the various Kuiper belt sub-populations to the H_g-magnitude corresponding to the break in the size distribution (at $H_g = 9.0$), the CFEPS $H_g < 9.16$ classical and resonant population estimates from Petit et al. (2011) and Gladman et al. (2012) were converted to $H_g < 9.0$ (which corresponds to diameter $d > 108$ km for a g-band albedo of 5%) population estimates with a minor multiplicative tuning of

$$\frac{N(< H_g = 9.0)}{N(< H_g = 9.16)} = 10^{(0.8(H_g - 9.16))} = 10^{(0.8(9.0 - 9.16))} = 0.745 \qquad (4)$$

For example, the $H_g = 9.16$ classical inner belt population estimate from Petit et al. (2011) of 3000, implies ≈ 2200 objects with $H_g = 9.0$.

2.2. Öpik collision probability code

To compute the impact probability onto the surface of Pluto we modified a version of the Öpik collision probability code based on Dones et al. (1999), which implements the method described in Wetherill (1967). The code numerically integrates the collision probability of two bodies by assuming uniform precession of the nodal longitude and argument of pericenter of both the impactor and target over their precession cycles. The program adapts the integration step when the probability integrand becomes large. Our implementation of this code uses the relative fraction of each Kuiper belt sub-population (described in Section 1.1.1) divided into a grid of a, e, i cells of size 1 AU, 0.05, and 2°, respectively. The code uses each grid entry as the orbit of a potential Pluto impactor. The collision probability computed for the orbit is multiplied by the fraction of the population in that cell. The code gravitationally focuses the collision probability, providing the impact probability (/yr/object) as well as the impact velocity spectrum (in km/s) of the modeled population, with Pluto's escape speed (1.2 km/s) added in quadrature. The motion of Pluto about the Pluto–Charon system barycenter (25 m/s) is neglected.

The Öpik collision probability code used in this study was modified to bin the collision probability for each orbital precession orientation into individual impact velocity bins (as opposed to computing an average impact velocity from all possible impact orientations over a full orbital precession of the nodes). This produces detailed impact velocity distributions for each Kuiper belt sub-population onto Pluto (Fig. 3).

As expected, each sub-population has a different impact velocity spectrum onto Pluto. Due to their large semimajor axes, unsurprisingly the scattering objects peak at the highest impact velocity of the Kuiper belt sub-populations. The classical inner objects have a bimodal impact velocity spectrum (with peaks at ≈ 2 km/s and ≈ 3.5 km/s) due to their bimodal inclination distribution which has a gap between roughly 7° and 20° (Petit et al., 2011). The remaining populations have unimodal distributions peaking somewhere between 1.6 km/s and 2.0 km/s, with tails out to beyond 5 km/s. The impact speed spectrum produced by Dell'Oro et al. (2013) from a model of collisionally evolving TNOs (extracted from the CFEPS L7 synthetic model) impacting the plutinos independently reproduces these same main trends shown in Fig. 3.

2.3. Impact rates onto Pluto

The Öpik collision probability code produces impact probabilities with Pluto (/yr/projectile) that turn into impact rates (/yr) after multiplying by the estimated number of projectiles in each sub-population. Table 1 gives sub-population types (sometimes with orbital element cuts), impact probabilities (/yr/object in the group), telescopic population estimates for $H_g < 9.0$, and impact rates (/yr) from $H_g < 9.0$ projectiles. The 42 AU pericenter cut for the classical main sub-populations corresponds to Pluto's maximum nodal distance (see Section 1.1.1). There are essentially no hot classical main objects with $q < 42$ AU. The scattering object (S.O.) 200 AU semimajor axis division is a useful boundary due to the fact that the $a > 200$ AU S.O.s spend most of their time far from Pluto and so have a small impact probability, as can be seen by the factor of ≈ 50 in impact probability between the $a < 200$ AU and $a > 200$ AU S.O.s in Table 1. There are also essentially no S.O.s with $a < 15$ AU, and, in any case, $a < 15$ AU scattering objects require eccentricity $e > 0.98$ to intersect Pluto.

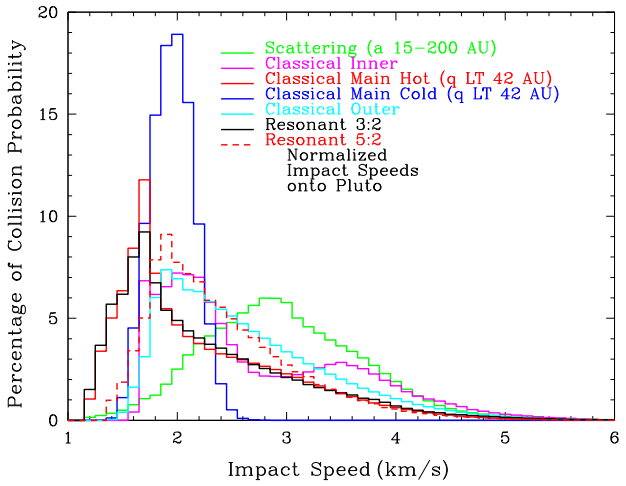

Fig. 3. Impact velocity spectrum onto Pluto for KRQ11 and CFEPS L7 Kuiper belt sub-populations. Escape speed from Pluto is 1.2 km/s. Each sub-population's distribution is separately normalized.

The Öpik collision probability code assumes uniform precession of Pluto's nodal longitude and argument of pericenter. There are methods that would help correct this assumption (Vokrouhlický et al., 2012; Pokorný and Vokrouhlický, 2013), but because Pluto experiences Kozai librations while also in the 3:2 mean-motion resonance with Neptune, its orbit neither uniformly precesses nor is it easily analytically modeled. In principle, the non-uniform precession could make important modifications to the impact rate. Our method to estimate the importance of this effect was to perform full N-body 100 Myr numerical integrations of the four outer planets and Pluto (resulting in Pluto performing its full dynamics) along with test-particle models of the CFEPS classical (inner, hot, stirred, kernel, and outer) and resonant 3:2 Kuiper belt sub-populations. We logged close encounters between Pluto and the KBOs and compared the number of close encounters logged in 100 Myr with the number expected from the Öpik code over this length of time. The Pluto dynamics correction factor in Table 1 accounts for this by providing the ratio of close encounters logged in these numerical integrations to that from the Öpik estimate. To provide enough logged close encounters in the integrations to reach 10% accuracy in the correction factors, both the numerical integrations and the Öpik estimate used for this purpose had a Pluto encounter radius of $R = 0.005$ AU ~ 625 Pluto radii. The corrected impact rates (/yr) shown in the second-to-last column of Table 1 account for the correction factors and should thus be used in future work. The last column of Table 1 shows the percentage of the total corrected impact rate for each sub-population.

As shown in Table 1, the effect of Pluto's Kozai dynamics, which causes its ecliptic nodal distances to always lie in the range $\simeq 33$—42 AU, is most important for the $q > 42$ AU stirred and kernel classical main objects, which have their impact rate drop by a factor of ≈ 5 and 2.5, respectively, when corrected. As a result, the impact rates for the $q > 42$ AU stirred and kernel classical main objects are each roughly an order of magnitude lower than the other populations that end up dominating the impact rate. The collision probability does not drop to zero due to the non-zero inclinations of some classical main KBOs. A curious phenomenon (as described in Section 1.1.1) regarding each of the $q < 42$ AU classical main sub-populations is the oscillation of Pluto's ecliptic nodal distance over the past 4 Gyr between $\simeq 33$ AU and $\simeq 42$ AU which causes its intersection with the main classical KBOs to also oscillate. When Pluto's nodal distance is between $\simeq 38$ AU and $\simeq 42$ AU, roughly in the middle of the $q < 42$ AU main belt population, its collision probability with the main classical KBOs increases. However, when Pluto's orbit intersects the ecliptic plane inside roughly 38 AU, the collision rate with the main classical KBOs drops due to the relative absence of such low-q objects. Surprisingly, the intersection oscillation between Pluto's orbit and the $q < 42$ AU classical main sub-populations due to Kozai results in the same impact rate onto Pluto as for the assumption that Pluto's orbit uniformly precesses (i.e., the correction factor = 1.0, to 10% accuracy). The $q < 42$ AU hot and stirred classical main objects compete with two other populations (see below) for the dominant impact flux onto Pluto. The classical outer objects (which in this study include the detached objects) mostly have $q < 42$ AU but, because their large semimajor axes keep them mostly at large distances from Pluto, they experience a similar balancing phenomenon (correction factor = 1.0) and we find that Pluto's Kozai oscillation contributes no appreciable correction to their impact rate onto Pluto. In contrast, the classical inner objects gain a non-negligible enhancement ($\approx 30\%$) in their collision probability with Pluto, because they entirely lie in the region where Pluto's ecliptic nodal distances always remain ($\simeq 33$—42 AU) (see Section 1.1.1).

Our study shows that the basic Öpik collision probability algorithm (not including Pluto's Kozai effect) also underestimates the impact rate of the plutinos (other 3:2 resonant KBOs) onto Pluto by $\approx 50\%$. In this case, our numerical integration had both the

Table 1
Öpik collision probability calculations. "Classical Main H" is the hot classical sub-population, "Classical Main S" is the stirred component of the cold classicals, and "Classical Main K" is the kernel component of the cold classicals (Petit et al., 2011). Impact probabilities are (/yr/object). Population estimates are for $H_g < 9.0$ (diameter $d > 108$ km, for a g-band albedo $p = 5\%$). Impact rates are (/yr) and determined using the number of $H_g < 9.0$ objects in each sub-population. Pluto dynamics correction factors (see text) are accounted for in the corrected impact rates (/yr) as well as the % of the total impact rate values. Bold values show the four sub-populations that dominate the total impact rate onto Pluto.

Kuiper belt sub-population type	Öpik impact probability (/yr/KBO)	$H_g < 9.0$ Population estimate	Öpik impact rate (/yr)	Pluto dynamics correction factor (0.1 accuracy)	Corrected impact rate (/yr)	% of Total impact rate
S.O. (15 AU $\leqslant a \leqslant$ 200 AU)	7.5e−17	8,000	6.0e−13		6.0e−13	1.3
S.O. ($a > 200$ AU)	1.4e−18	72,000	1.0e−13		1.0e−13	0.2
Classical inner	3.9e−16	2,200	8.6e−13	1.3	1.1e−12	2.3
Classical Main H ($q < 42$ AU)	4.4e−16	26,000	1.1e−11	1.0	1.1e−11	**23.0**
Classical Main S ($q < 42$ AU)	4.0e−16	30,000	1.2e−11	1.0	1.2e−11	**25.1**
Classical Main S ($q > 42$ AU)	4.4e−16	18,000	7.9e−12	0.2	1.6e−12	3.4
Classical Main K ($q < 42$ AU)	4.3e−16	8,300	3.6e−12	0.9	3.2e−12	6.7
Classical Main K ($q > 42$ AU)	4.0e−16	4,700	1.9e−12	0.4	7.6e−13	1.6
Classical outer	1.0e−16	60,000	6.0e−12	1.0	6.0e−12	**12.6**
Resonant 3:2	5.9e−16	10,000	5.9e−12	1.5	8.9e−12	**18.6**
Resonant 2:1	3.3e−16	2,700	8.9e−13	~ 1	8.9e−13	1.9
Resonant 5:2	1.8e−16	9,000	1.6e−12	~ 1	1.6e−12	3.3
Total					4.8e−11	100.0

plutinos and Pluto in the 3:2 mean-motion resonance and some plutinos also undergoing Kozai. The net result is a mild (50%) increase of the impact rate due to the enhanced frequency of low-velocity encounters caused by a greater frequency of close orbital alignments. Even without the 50% correction factor, the plutinos are comparable to the impact flux of the other three dominant populations. The correction factors for the resonant 2:1 and 5:2 populations were not measured using numerical integrations, but we do not expect them to modify the Öpik approximation to $> 10\%$ accuracy; in any case they are comparable to each other but down by roughly an order of magnitude from the dominant populations. We did not include other resonant populations in our analysis, because their contributions to Pluto's impact flux will be small compared with the nearby and more numerous 2:1 and 5:2 populations (Gladman et al., 2012). The reader may be surprised that the scattering object impact flux onto Pluto is currently small, contributing only $\approx 2\%$ of the total impact flux. Thus, Pluto is dominantly hit by a wider variety of Kuiper belt sub-populations than the satellites of Jupiter and Saturn, particularly by the cold classical objects which do not reach into the giant planet region.

Examining all the Kuiper belt sub-populations, Table 1 shows that one is faced with the complication that no single population dominates the impact flux onto Pluto. In fact, the $q < 42$ AU hot and stirred classical main, the classical outer (which include the detached objects), and the plutino populations each provide roughly comparable (15—25%) contributions to the total impact flux, together outweighing the sum of all other sub-populations by roughly a factor of four. Computing impact rates and thus cratering rates onto the surface of Pluto using only a model of the cold classical Kuiper belt objects thus underestimates the age of Pluto's surface, although this depends of course on the number of KBOs assumed in the classical belt.

In detail we find that our total impact rate of 4.8×10^{-11}/yr is a factor of ≈ 2.5 less than estimated by Durda and Stern (2000) for $d > 100$ km impactors, who found an impact rate of $\approx 1.2 \times 10^{-10}$/yr assuming 70,000 KBOs greater than this size (see their Fig. 6). Zahnle et al. (2003) found an estimated impact rate onto Pluto of 2.3×10^{-11}/yr (within a factor of 2) for $d > 100$ km impactors scaled from the calculations of (Nesvorný et al., 2000) for plutino impacts on Pluto and from an Öpik-style estimate from W. Bottke (private communication) and using 38,000 KBOs of this size. Our total impact rate of 4.8×10^{-11}/yr for $d > 100$ km impactors agrees within their uncertainty, even with our change in population estimates and our use of an impact velocity spectrum (which is used to gravitationally focus the Öpik impact probabilities computed for each target and projectile orbital precession orientation) rather than an average impact velocity. More important to the interpretation of the New Horizons crater density observations is that our production of an impact speed distribution allows us to examine its influence on Pluto's cratering rates, which have velocity dependence in the crater scaling law.

The recent paper by Bierhaus and Dones (2015) found that the cold classical main objects (with stirred and kernel sub-components) contribute $\approx 70\%$ and $\approx 99\%$ of the projectile flux onto Pluto for $d > 10$ km and $d > 1$ km, respectively. This is primarily due to their use of a steeper slope ($\alpha_{faint} = 0.38$) for the cold classical main objects compared with the hot classical main objects ($\alpha_{faint} = 0.2$), citing Fraser et al. (2014). This steeper faint-end slope for the cold classicals compared with the hot classicals causes their contribution to increasingly dominate Pluto's total impact flux for smaller and smaller impactor sizes. In this paper, we assume all sub-populations have $\alpha_{faint} = 0.4$ since the $\alpha_{faint} = 0.38$ $(+0.05, -0.09)$ slope for cold classicals is much better determined than the proposed $\alpha_{faint} = 0.2$ $(+0.1, -0.6)$ for hot classicals (uncertainties quoted from Fraser et al. (2014)). For the bright end of the size distribution, Bierhaus and Dones (2015) use the slopes for the hot and cold classicals from Fraser et al. (2014) ($\alpha_{bright} = 0.87$ and $\alpha_{bright} = 1.5$, respectively). Our use of $\alpha_{bright} = 0.8$ instead for all Kuiper belt sub-populations has little effect on conclusions about crater densities because we will show that $D > 400$ km craters formed in the last 4 Gyr are absent, and thus only the total number of $d > 100$ km projectiles is relevant in order to establish the absolute calibration linked to observed KBOs.

2.3.1. Uncertainties in the total impact rate

The uncertainty in our total impact rate comes from a variety of factors. The Öpik impact rate (/yr) depends on the accuracy of the population estimates used for each Kuiper belt sub-population. The absolute calibration for scattering objects (Kaib et al., 2011) is based on only 11 known objects (Shankman et al., 2013), contributing an uncertainty in the population estimate of $1/\sqrt{N} = 30\%$; however, the scattering objects contribute only a small fraction ($\approx 2\%$) to Pluto's impact flux. Uncertainties for the CFEPS classical and resonant population estimates are given in Petit et al. (2011) and Gladman et al. (2012), respectively. As the four dominating sub-populations for the impact flux onto Pluto, the population estimates for the $q < 42$ AU hot and stirred classical main objects have an uncertainty of roughly 25%, the classical outers roughly 75%, and the plutinos roughly 45%. Lastly, we aimed to have our Pluto dynamics correction factors good to 10% accuracy. Overall, we estimate a $\pm 50\%$ uncertainty in our total impact rate shown in Table 1. To determine the uncertainty in how the impact rate translates to a cratering rate, one must understand the cratering physics and the caveats discussed in Section 2.4.

2.4. Cratering rates onto Pluto

Because our analysis extends to include the impact speed distribution, there is not a simple one-to-one correspondence between impact rate and *crater formation rate larger than a given diameter threshold*. In order to convert impact rates (/yr) into primary cratering rates (/yr), we need to know the speed distribution and the differential size distribution for the individual populations (Gallant et al., 2009), which for the CFEPS model was expressed as $dN/dH \propto 10^{\alpha H_g}$ for $H_g < 9$. There are several estimates for where a break in the H_g-magnitude size distribution occurs and how the distribution is extrapolated to small diameters (Jewitt et al., 1998; Gladman et al., 2001; Bernstein et al., 2004; Fraser and Kavelaars, 2008; Fuentes and Holman, 2008; Shankman et al., 2013; Adams et al., 2014). We simply adjust the CFEPS L7 population estimates from $H_g = 9.16$ down to a break at $H_g = 9.0$, and then follow the analysis of Shankman et al. (2013) who placed a knee or divot at $H_g = 9.0$. We normalize the size distributions to the number of objects with $H_g < 9.0$ as listed in Table 1.

For the first time in the literature, we compute primary cratering rates using the impact speed distribution for each given Kuiper belt sub-population (see Fig. 3), looping over the velocity bins. Starting with the lowest velocity bin, the needed impactor diameter to create a crater of a desired size is computed using the simple-to-complex crater scaling laws from Zahnle et al. (2003):

$$D_s = 11.9 \left(\frac{U^2}{g}\right)^{0.217} \left(\frac{\delta}{\rho}\right)^{0.333} \left(\frac{d}{\text{km}}\right)^{0.783} \text{km} \tag{5}$$

and then

$$D = \begin{cases} D_s & \text{for } D_s < D_{tr} \quad \text{(a)} \\ D_s (D_s/D_{tr})^{\xi} & \text{for } D_s > D_{tr} \quad \text{(b)} \end{cases} \tag{6}$$

where U is the impact velocity (in km/s), d is the impactor diameter, and the gravitational acceleration on the surface of Pluto is

$g = 64.0\ \mathrm{cm/s^2}$. We assume both impactor δ and target ρ (at surface) densities are $\delta = \rho = 1.0\ \mathrm{g/cm^3}$. To accommodate the transition from simple (D_s) to complex (D) craters, we assume the transition diameter $D_{tr} \simeq 4$ km on Pluto (Moore et al., 2014), and $\xi = 0.108$ (McKinnon and Schenk, 1995).

It is important to note that our cratering calculations assume a water–ice surface, and that for the case of craters formed entirely in solid N_2 (similar density) or CH_4 (lower density) the simple crater diameter D corresponding to a given impactor diameter d would shift by up to 24% (for a CH_4 density of $0.52\ \mathrm{g/cm^3}$ (Lupo and Lewis, 1980)).[5] Contrary to icy bodies such as the saturnian satellites, because impact velocities can be as low as 1–2 km/s, the Pluto system has a crater scaling of (roughly) only 3–7 times the impactor's diameter, compared with ~ 10—20 times as is common elsewhere in the Solar System (Dones et al., 2009).

The slightly different crater scaling law from Housen and Holsapple (2011) (and used by Bierhaus and Dones (2015), their Eq. (1)), was developed from laboratory experiments studying the ejecta (and thus secondaries) produced during the crater formation process into sand-like material. This crater scaling law results in approximately 3% smaller simple crater diameters than those computed from the crater scaling laws (Eqs. (5), (6a), and (6b)) in Zahnle et al. (2003), developed for solid, non-porous geological materials. The lower limit on cratering efficiency is given by porous, "sand-like" scaling, which gives somewhat smaller craters overall. The scaling in Housen and Holsapple (2011) (and used by Bierhaus and Dones (2015)) could apply to the smallest craters likely to be seen on Pluto or Charon, those formed entirely within an icy regolith, which will slightly affect the slope of the crater production function, all other things being equal, unless saturation occurs at the scales in question, in which case it will not matter. For the broad range of crater sizes we discuss in this paper, the crater scaling laws from Zahnle et al. (2003) that include the simple-to-complex transition are applied.

A caveat to applying these equations to the Pluto system is that the physics of crater creation and the crater scaling laws have been studied mostly for the icy galilean and saturnian satellites. For these bodies, typical impact speeds range from 10 to 20 km/s (hypervelocity), because orbital speeds are higher and impactors get more gravitational focusing from the giant planets than in the Kuiper belt, where impact speeds are typically 1–2 km/s (potentially sub-hypervelocity). High-e scattering objects at perihelion also travel at higher orbital speeds than the lower-e classical and resonant populations located in the Kuiper belt. For this reason, applying crater scaling laws developed for the icy satellites of the giant planets to craters on Pluto may imprecisely convert impact rates into cratering rates. However, given that the crater scaling law has not been rigorously developed at slower impact speeds (except for sand and water (Schmidt, 1980)), the best way forward is to apply the above crater scaling laws. In addition, Singer et al. (2013) (their Appendix A) argue that existing scaling laws may be extrapolated to even lower speeds (those of secondary crater formation) as long as the Hugonoit elastic limit is exceeded, which is well satisfied for primary impacts on Pluto and Charon.

Once the needed impactor diameter d to create a crater of a desired threshold diameter D at the minimum impact speed (Pluto's escape speed) is computed, this d is converted to a H_g-magnitude using Eq. (1), assuming a g-band albedo p of 5%. By integrating down the size distribution which is pegged at $H_g = 9.0$ for the population estimates shown in Table 1, the number of objects less than the impactor H_g-magnitude ($N(< H_g)$) is computed. Because we have an impact speed distribution rather than a single impact velocity, we must then repeat this process for each subsequently larger velocity bin. By progressing through the impact speed distribution, slightly higher impact speeds correspond to slightly smaller impactor diameters d for creating a fixed crater diameter D. This means that as we compute $dN(H_g)$ for progressively smaller impactors we add the number of additional smaller objects to the total number of objects which can create the desired crater size. The number of additional objects added for each subsequent velocity bin is multiplied by the fraction of the velocity distribution with v greater than the current velocity bin before it is added to the cumulative number of objects for the desired crater size.

Once the above process is completed out to $v_{impact} = 6$ km/s (the effective end of the tail of the distribution), the cumulative number of impactors that can make a crater larger than the desired crater threshold is multiplied by the impact probability (/yr/object) given in Table 1 and corrected by the "Pluto dynamics correction factor" also given in Table 1. The output is the current primary cratering rate (/yr) onto Pluto for the modeled Kuiper belt sub-population and a desired threshold crater diameter D. Note that this is more-or-less a direct calculation of the cumulative impact rate, and should be equivalent to the Monte Carlo approach used by Zahnle et al. (1998) to calculate the differential impact rates on planetary satellites from assumed cometary orbital distributions. We first repeated this process three times to study the variation in how the impactor differential H_g-magnitude size distribution might extend to $d < 100$ km, using three extrapolation scenarios (Fig. 2): a single power-law with logarithmic slope $\alpha = 0.8$ ($q_{slope} = 5$); a power-law with a sudden knee at $H_g = 9.0$, slope $\alpha_{bright} = 0.8$ on the bright side of the knee, and slope $\alpha_{faint} = 0.4$ ($q_{faint} = 3$) on the faint side of the knee; and thirdly a power-law with a "divot" at $H_g = 9.0$ with the same α_{bright} and α_{faint} as the knee scenario, but with a contrast (ratio of the number of objects in the population just bright of the divot to the number of objects just faint of the divot) value of $c = 6$ (Shankman et al., 2013).

Table 2 shows the current cratering rate onto Pluto for 5 different sample threshold crater diameters and these three impactor size distribution scenarios (SPL/knee/divot), with the total cratering rates in the last row. The single power-law is somewhat of a strawman and is used for illustrative purposes of a very steep size distribution extending down to km-scale. The 400-km-diameter crater case corresponds roughly to a 100-km-diameter impactor travelling at 2 km/s, thus estimating the cratering rate at roughly the break in the impactor differential size distribution. For each population this crater diameter gives roughly the same current cratering rate for all three size distribution scenarios; they are not identical because some smaller "post-break" KBOs in the high-speed tail intrude into the $D \geqslant 400$ km regime. The 100-km-diameter crater case is roughly at the limit for which we do not expect any craters of this size or larger to exist on Pluto over 4 Gyr (at *current* rates). Dropping down in scale to $D \geqslant 30$ km craters, one begins probing the size distribution beyond the break where the SPL cratering rates are roughly a factor of 250 higher than for the size distribution with a knee. The factor of ≈ 6 between the knee and divot cratering rates reflects the value of 6 used for the contrast c. The deviation of the SPL from the knee size distribution of course increases for still-smaller crater diameters. Thirty-km-diameter and smaller craters should be observed by New Horizons, even if Pluto is as geologically active in degrading and erasing craters as Triton (Young et al., 2008; Moore et al., 2014).

2.5. Number of craters on Pluto's surface

The cratering rates (/yr) given in Table 2 are for the *current* census of each sub-population of Kuiper belt objects. It is thought each

[5] In addition, the simple-to-complex transition in these weak materials may occur at a smaller diameter, increasing the size of a complex crater over that given in Eq. (6b). Whether any impacts in volatile N_2 and CH_4 ice can long survive on Pluto's surface is an open question (Stern et al., 2015).

Table 2
Current primary cratering rates onto Pluto using our derived impact velocity distribution for each Kuiper belt sub-population and three impactor size distribution scenarios: a single power-law (SPL) (top), a knee (middle), and a "divot" (bottom) for 5 sample crater-diameter-thresholds. Cratering rates are computed from corrected impact probabilities in Table 1. This table should not be used for surfaces expected to be greater than a few hundred Myr old.

Kuiper belt sub-population type	Current cratering rate, $D \geqslant 400$ km (/yr) SPL/knee/divot	Current cratering rate, $D \geqslant 100$ km (/yr) SPL/knee/divot	Current cratering rate, $D \geqslant 30$ km (/yr) SPL/knee/divot	Current cratering rate, $D \geqslant 10$ km (/yr) SPL/knee/divot	Current cratering rate, $D \geqslant 3$ km (/yr) SPL/knee/divot
S.O. (15 AU $\leqslant a \leqslant$ 200 AU)	2e−12	9e−10	2e−7	4e−5	1e−2
	1e−12	5e−11	7e−10	9e−9	2e−7
	7e−13	8e−12	1e−10	2e−9	3e−8
Classical inner	2e−12	2e−9	4e−7	6e−5	2e−2
	2e−12	7e−11	1e−9	2e−8	3e−7
	1e−12	1e−11	2e−10	3e−9	4e−8
Classical Main H ($q < 42$ AU)	2e−11	1e−8	3e−6	4e−4	1e−1
	1e−11	6e−10	1e−8	1e−7	2e−6
	1e−11	1e−10	2e−9	2e−8	4e−7
Classical Main S ($q < 42$ AU)	1e−11	7e−9	2e−6	3e−4	8e−2
	1e−11	6e−10	9e−9	1e−7	2e−6
	1e−11	1e−10	2e−9	2e−8	3e−7
Classical Main S ($q > 42$ AU)	1e−12	8e−10	2e−7	3e−5	1e−2
	1e−12	7e−11	1e−9	2e−8	3e−7
	1e−12	1e−11	2e−10	2e−9	4e−8
Classical Main K ($q < 42$ AU)	3e−12	2e−9	5e−7	7e−5	2e−2
	3e−12	2e−10	2e−9	3e−8	5e−7
	3e−12	3e−11	4e−10	5e−9	9e−8
Classical Main K ($q > 42$ AU)	7e−13	4e−10	1e−7	2e−5	5e−3
	7e−13	4e−11	6e−10	7e−9	1e−7
	7e−13	6e−12	1e−10	1e−9	2e−8
Classical outer	1e−11	7e−9	2e−6	3e−4	9e−2
	1e−11	4e−10	7e−9	8e−8	1e−6
	7e−12	7e−11	1e−9	1e−8	2e−7
Resonant 3:2	1e−11	8e−9	2e−6	3e−4	1e−1
	1e−11	5e−10	8e−9	1e−7	2e−6
	8e−12	9e−11	1e−9	1.7e−8	3e−7
Resonant 2:1	1e−12	7e−10	2e−7	3e−5	8e−3
	1e−12	5e−11	8e−10	1e−8	2e−7
	8e−13	9e−12	1e−10	2e−9	3e−8
Resonant 5:2	3e−12	2e−9	4e−7	6e−5	2e−2
	2e−12	9e−11	2e−9	2e−8	3e−7
	2e−12	2e−11	3e−10	3e−9	6e−8
Total	7e−11	4e−8	1e−5	2e−3	5e−1
	6e−11	3e−9	4e−8	5e−7	9e−6
	5e−11	5e−10	7e−9	9e−8	2e−6

of these sub-populations have naturally dynamically depleted with time at differing rates over the last ≈ 4 Gyr, so in order to convert the cratering rates into the cumulative number of craters on Pluto's surface, we used theoretically estimated decay rates for each Kuiper belt population and integrated backwards in time to determine the enhancement. The time period we feel that can be reliably studied is Pluto's post-installation phase from 3.9 Gyr ago to the present day, where it is reasonable to assume only the number of projectiles in each population has changed, but the orbital distributions have remained the same because the Solar System architecture has not changed. We use the functional form:

$$\frac{N(t)}{N_0} = \left(\frac{4.5\ \text{Gyr}}{t}\right)^b, \quad 0.5 < t < 4.5\ \text{Gyr} \tag{7}$$

for the decay rate of each Kuiper belt sub-population, where $N(t)$ is the number of objects in the population at some time t measured in Gyr forward from 4.0 Gyr ago, N_0 is the number of objects in the population today at $t \approx 4.5$ Gyr (see Table 1). The value of b is estimated from Kuchner et al. (2002), Hahn and Malhotra (2005), and Lykawka and Mukai (2005) for the classical Kuiper belt objects (where we take $b = 0.1$), from Morbidelli (1997) and Tiscareno and Malhotra (2009) for the resonant 3:2 objects ($b = 0.52$), from Tiscareno and Malhotra (2009) for the resonant 2:1 objects ($b = 0.77$), and from Hahn and Malhotra (2005) for the resonant 5:2 objects ($b = 0.05$). The scattering objects are estimated for the time period 100 Myr $< t <$ 4 Gyr using the data from Dones et al. (2004) directly (their Fig. 8), because a power-law does not represent the simulations well. A power-law of the form $N(t) \propto t^{-b}$ with $b \sim 0.7$ for the time period 9 Myr $< t <$ 4 Gyr approximately fits the decay (L. Dones, private communication, 2014), but only fits well at the end-points of the data so we chose to use the simulation results directly to compute the enhancement.

The enhanced bombardment factor (EBF) shown in Table 3 was computed by integrating the above functional form (Eq. (7)) over the past 4 Gyr ($t \approx 0.5$—4.5 Gyr), comparing the integrated number of objects over the past 4 Gyr to that of a constant population. The EBF is thus a scaling factor needed to account for the decay of each Kuiper belt sub-population over the past 4 Gyr. It should be interpreted as the cumulative number of depleting objects in the past being equivalent to a constant population over the last 4 Gyr that is some multiplicative factor more than the current population. For example, the b value for the plutinos implies that this population was ≈ 3.2 times as populous 4 Gyr ago as it is today (from Eq. (7)); its EBF of 1.53 means the integrated number of impacts from the decaying population over the age of the Solar System is equivalent to that from a constant population 1.53 times larger than today's.

Table 3 presents the number of craters larger than a given threshold crater diameter D obtained by multiplying Table 2's cratering rates by 4 Gyr and the EBF for each sub-population. For example, the number of craters with $D \geqslant 30$ km generated by the plutinos for a divoted impactor size distribution was found the following way: $(1 \times 10^{-9}) * (4 \times 10^{9}) * (1.53) = 8$ craters.

We find that the 3:2 resonant population is the largest single contributor to the integrated collisional history onto Pluto, accounting for about a quarter of its impact craters over the last 4 Gyr. Compared with the other three competing populations that provide major contributions to Pluto's current impact flux (the $q < 42$ AU hot and stirred classical main objects and the classical outer objects), the 3:2 objects have decayed the most over the past 4 Gyr, making them more dominant than these impactor population contributions when integrated over Pluto's post-installation phase. Even with an EBF of 4.9, the scattering objects contribute little to Pluto's collisional history over the last 4 Gyr, only contributing roughly half as much as each of the $q < 42$ AU hot and stirred classical main objects and the classical outer objects. Thus, strictly speaking, the population of bodies that have cratered Pluto and Charon over the past 4 Gyr include a wider variety than those that impacted the giant-planet satellites. In particular, Pluto and Charon have been impacted by the cold classical belt objects in addition to the hot populations (the scattering objects, hot classical objects, and the resonant populations) whereas the cold classicals do not reach far enough into the giant planet region to impact the outer Solar System satellites. Although the scattering objects and the plutinos may have been drawn from the same parent population long ago and thus show the same size distribution, the cold classical belt might have a different break point, and is known to have a steeper $H_g < 9$ slope (e.g., (Petit et al., 2011; Fraser et al., 2014; Adams et al., 2014)), which together with its redder colors (Doressoundiram et al., 2008; Sheppard, 2012) make it a separate population from the scattering, resonant, and hot classical Kuiper belt objects, possibly in situ in origin. It is also interesting to note that Table 3 indicates there is only a $20-30\%$ chance that Pluto has even one impact basin ($D > 400$ km formed by $d \gtrsim 100$ km impactors) formed in the current (i.e. post-installation) impacting environment.

3. Discussion

We anticipate that the interpretation of the cratering record will be fraught with complications, as we now describe.

3.1. Interpretation of young surfaces

If New Horizons finds a surface that appears "lightly-cratered" or "young" (especially if portions of Pluto or Charon have low crater densities similar to Triton), then one would first compute a crater retention age using the "current day" cratering rates given in Table 2. With very young regions there is always the difficulty of being sure one is selecting a region with a single coherent re-surfacing age, but let us assume this could be done. If the calculated age is small enough that the decay of the impactor populations is not a concern (roughly a few hundred million years), then the uncertainty on this derived age will depend essentially entirely on the assumption of which extrapolation one prefers for projectiles smaller than the break diameter in the impactor size distribution. Our calculations show that unless the single power-law impactor size distribution or some other steep size–frequency distribution (SFD) (e.g., cases A and B in Zahnle et al. (2003) and Schlichting et al. (2013)) actually were the correct model, all cratered surfaces will be unsaturated over the last 3.9 Gyr for $D > 1$ km. Melosh (1989), Eq. (10.2.10), shows saturation occurs when the cumulative crater density $N_{cs} = 1.54D^{-2}$ or the relative crater frequency $R = 3.12$. As an example, Fig. 4 shows the cumulative number of craters per square km that are larger than several threshold crater diameters D versus the crater retention age of a surface on Pluto. If the crater density of $D \geqslant 3$ km craters on a young surface were to be $10^{-4.5}$ km^{-2}, then one would conclude a retention age of ≈ 100 Myr if the knee model is the best representation of the size distribution; in contrast, if the power-law break located up at impactor diameters of 100 km is a divot, this same surface would require nearly ≈ 600 Myr of exposure to reach the same crater density. At small crater diameters the influence of the relatively tiny number of projectiles larger than the impactor power-law break diameter is irrelevant and this age ratio is essentially the contrast at the transition diameter. So, how can one know which (if any) assumption/distribution is valid?

3.2. The issue of the size distribution below the break

At first glance, one might hope that Pluto's crater record will itself provide information that resolves the uncertainty in the behavior of the size distribution near the power-law break diameter, for without this resolution the factor-of-six is inherent and dwarfs all other uncertainties in the problem for the case of a single-slope extrapolation of the impactor size distribution to sub-km sizes. Unfortunately, our calculations show that over the last ≈ 4 Gyr, Pluto is unlikely to have been struck by even a single impactor with a diameter larger than the break ($d \approx 100$ km, $D \approx 400$ km; see Table 3), so on *any* surface that post-dates Pluto's installation onto its current orbit (if any exist) we expect to see only craters caused by the projectiles smaller than 100 km in diameter.

However, if any young surfaces are visible upon arrival in the Pluto system, those young surfaces should record the slope or slopes of the size distribution over the range of visible craters. For example, if the entire surface of Pluto appears, like Triton, to be relatively young, then the existing craters will reflect the size–frequency distribution (SFD) of the production population (at least, down to the diameter where pollution by secondaries (Section 3.5) begins). In particular it should be trivial to differentiate between, e.g., the single power-law size distribution with $\alpha \simeq 0.8$ ($q \simeq 5$) and a shallower slope of $\alpha_{faint} \sim 0.4$ ($q_{faint} \sim 3$), most likely measured using craters in the 1–100 km diameter range. While finding the shallower of these two slopes would rule out the steep $\alpha_{bright} = 0.8$ power-law continuing uninterrupted from the break diameter down to impactors in the sub-km-scale range, measuring an $\alpha_{faint} = 0.4$ does not resolve the question of how that connects to the well-measured and absolutely-calibrated projectile population with $d > 100$ km. Our estimates (Table 3) show that we do not expect the changing shape caused by the impactor distribution near the break (expected to be recorded only in the 200–500 km crater diameter range) to exist in post-installation terrains. This is illustrated in Fig. 5, which shows the cumulative crater density for craters larger than a threshold diameter D for the knee and divot impactor size distribution extrapolation scenarios for different surface ages. The solid black line in Fig. 5 is the crater equilibrium curve from Melosh (1989), his Fig. 10.2, which is $0.07N_s$ or approximately $R = 0.2$ in that figure. The horizontal dashed line at -7.2 corresponds to 1 crater/Pluto surface, meaning any finite crater density below this line will not be realized on Pluto in the last 4 Gyr. Thus, one cannot use the size distribution of craters present on "younger" terrains to differentiate between the knee and divot scenarios.

This being the case, obtaining better than "factor-of-six" crater retention ages in the Pluto system from our models will require one of two resolutions. First, future observations of the Kuiper belt

Table 3
Cumulative number of craters over the past ≈ 4 Gyr on the surface of Pluto for 5 sample crater diameters for the three impactor size distribution scenarios (SPL/knee/divot) given in Table 2. EBF stands for the enhanced bombardment factor that is the scaling needed to account for the decay of each sub-population over the past 4 Gyr.

Kuiper belt sub-population type	EBF	Crater number $D_{crater} \geqslant 400$ km SPL/knee/divot	Crater number $D_{crater} \geqslant 100$ km SPL/knee/divot	Crater number $D_{crater} \geqslant 30$ km SPL/knee/divot	Crater number $D_{crater} \geqslant 10$ km SPL/knee/divot	Crater number $D_{crater} \geqslant 3$ km SPL/knee/divot
S.O. (15 AU $\leqslant a \leqslant$ 200 AU)	4.9	3e−2	18	5000	7e+5	2e+8
		3e−2	0.9	10	2e+2	3e+3
		1e−2	0.1	2	3e+1	5e+2
Classical inner	1.08	1e−2	6	2000	3e+5	8e+7
		9e−3	0.3	5	7e+1	1e+3
		5e−3	0.06	0.8	1e+1	2e+2
Classical Main H ($q < 42$ AU)	1.08	7e−2	40	10000	2e+6	5e+8
		6e−2	3	40	5e+2	9e+3
		4e−2	0.5	7	9e+1	2e+3
Classical Main S ($q < 42$ AU)	1.08	5e−2	30	8000	1e+6	4e+8
		5e−2	2	40	5e+2	9e+3
		5e−2	0.5	7	8e+1	1e+3
Classical Main S ($q > 42$ AU)	1.08	6e−3	4	900	2e+5	4e+7
		6e−3	0.3	5	6e+1	1e+3
		6e−3	0.06	0.8	1e+1	2e+2
Classical Main K ($q < 42$ AU)	1.08	1e−2	8	2000	3e+5	9e+7
		1e−2	0.6	10	1e+2	2e+3
		1e−2	0.1	2	2e+1	4e+2
Classical Main K ($q > 42$ AU)	1.08	3e−3	2	500	8e+4	2e+7
		3e−3	0.2	3	3e+1	5e+2
		3e−3	0.03	0.4	5e+0	9e+1
Classical outer	1.08	5e−2	30	8000	1e+6	4e+8
		5e−2	2	30	4e+2	6e+3
		3e−2	0.3	5	6e+1	1e+3
Resonant 3:2	1.53	8e−2	50	10000	2e+6	6e+8
		7e−2	3	50	6e+2	1e+4
		5e−2	0.5	8	1e+2	2e+3
Resonant 2:1	1.94	9e−3	5	1000	2e+5	6e+7
		8e−3	0.4	6	8e+1	1e+3
		7e−3	0.07	1	1e+1	2e+2
Resonant 5:2	1.04	1e−2	6	2000	3e+5	8e+7
		1e−2	0.4	6	8e+1	1e+3
		7e−3	0.07	1	1e+1	2e+2
Total		0.3	200	50000	8e+6	3e+9
		0.3	10	200	3e+3	5e+4
		0.2	2	40	4e+2	8e+3

that carefully probe the $d = 10$—100 km impactor size range ($H_g = 9$—14) should directly establish the number distribution of the current projectile population in an absolutely-calibrated way. This is most likely to be done first for populations whose members come to the smallest heliocentric distances (allowing detection of the smaller objects when they are at perihelion); meaningful improvements are most likely to be made in the near future by continuing to study the scattering objects (for which studies in the range $H_g = 9$—13 are already possible (Shankman et al., 2013; Adams et al., 2014)) or even more likely in the more plentiful plutino population (for which deeper surveys can probe down to $H_g \approx 11$ at the 28 AU perihelion of this population) (Alexandersen et al., 2014). While there currently are thus fragments of the observed size distributions across the outer Solar System small body populations, the entire diameter range is needed to make definitive statements about crater retention ages on the surfaces of Pluto and its moons.

Secondly, failing direct study of the current impactor population, it may be possible to at least detect the presence of the divot in Pluto's or Charon's cratering record itself. Because the current cratering rate is so low, we conclude the divot could only be visible on surfaces that *predate* the Pluto–Charon binary installation in the current Kuiper belt architecture. This could permit $D \sim 200$—400 km craters (which we shall term "basins") that are caused by $d = 50$—100 km impactors under the current bombardment to be present on ancient surfaces.

What would be the signature on the crater distribution as the bombardment accumulates to the point where the power-law break diameter's craters become present? The most obvious manifestation of this will be in the number of basins present relative to the number *expected* by extrapolation of the $D < 100$ km craters to larger diameters; this produces very different behavior in the knee and divot scenarios as illustrated in Fig. 2. This can also be seen in Fig. 5 of the cumulative crater density. In Fig. 5, the sharp power-law break present in Fig. 2 has smoothed out to a broader slope change due to both the cumulative nature of this plot and the width of the impact velocity spectrum. The peak of the divot, for example, is still at $D \approx 400$ km, but the slope change manifests itself over a broad range of crater diameters ($D \approx 100$ km to $D \approx 600$ km). Working from small projectiles up in Fig. 2, the small craters follow the shallow slope of the $\alpha_{faint} = 0.4$ ($q_{faint} = 3$) impactor distribution, but upon reaching a knee, the slope changes to a much steeper $\alpha_{bright} = 0.8$ ($q_{faint} = 5$) large-impactor distribution which results in considerably *fewer* basins than the extrapolation of the shallower power-law would detect. In contrast, in a divot scenario there is a sudden *excess* of projectiles in the $d = 100$—200 km range, and so there would be far more basins present than an extrapolation of the small craters would estimate. The

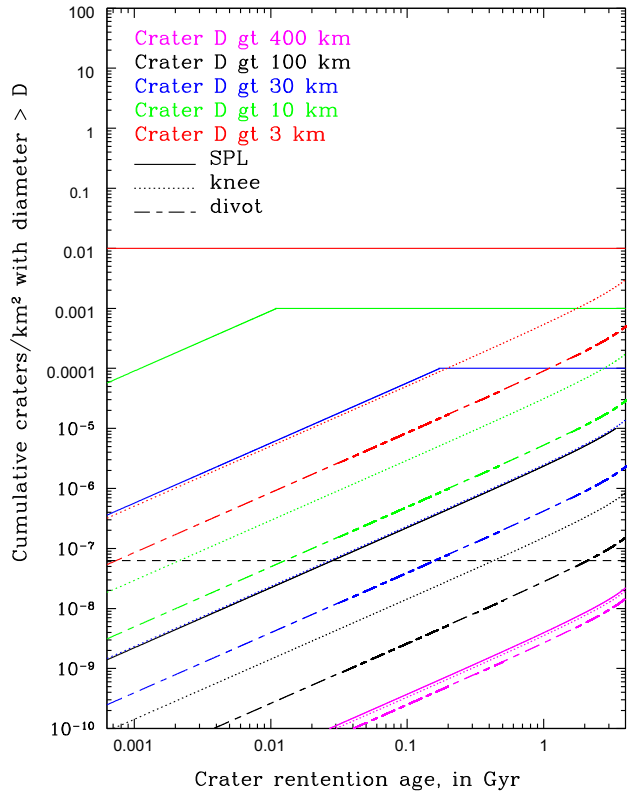

Fig. 4. Logarithm of primary crater density (# craters/km^2) on Pluto's surface versus age (Gyr) since last surface reset for 5 crater diameters and three impactor size distribution scenarios. For a given crater diameter, the inferred crater retention age can vary widely depending on assumptions of the size distribution. The horizontal line at −7.2 corresponds to 1 crater/Pluto surface. Note that the $D \geqslant 100$ km crater curve for the SPL nearly overlaps the $D \geqslant 30$ km crater curve for the knee scenario. Some SPL curves cease to rise above the empirically determined saturation level for the diameter in question (Melosh (1989); his Fig. 10.2). The dynamical depletion of the Kuiper belt sub-populations can be seen for crater retention ages near 4 Gyr.

horizontal line in Fig. 5 at −7.2 corresponds to 1 crater/Pluto surface. If the *pre*-installation bombardment is factors of many larger, and preserved, then this signal of a knee vs a divot will become accessible on Pluto's surface. This sudden basin excess is represented by a positive slope on a relative crater frequency (R) plot normalized to a differential D^{-3} distribution as is shown in Fig. 6 (Arvidson et al., 1979). The horizontal dashed line in Fig. 6 refers to the approximate empirically observed level of crater saturation on various Solar System bodies (see Melosh (1989), chapter 10, Fig. 10.2). The black squares correspond to 1 crater/Pluto surface on a cumulative plot, so unfortunately nothing to the right of those dots is expected to be visible on Pluto's post-installation terrains. Many times the current integrated bombardment rate would be needed from Pluto's *pre*-installation period to move the basin signal to the visible diameter range on Pluto.

In fact, we postulate that such a basin-excess feature has already been observed on Saturn's large moon Iapetus. Iapetus has been geologically inactive for its observable history; this and its distance from Saturn make Iapetus the best template to potentially record ancient Kuiper belt (scattering object) impacts. Dones et al. (2009) demonstrate that craters of this $D > 400$ km scale are more than an order of magnitude more abundant than extrapolation of current impact rates (based on small impactors (their Fig. 19.5 and Table 19.4)) suggests. This is also illustrated in Fig. 7 using relative crater densities from Kirchoff and Schenk (2010), where the R-values for basins of $D \approx 400$ km are clearly substantially larger than those in the 100-to-400 km diameter range, and is statistically consistent with the Shankman et al. (2013) divot in the scattering object impactor population. Using the crater scaling law of Eqs. (5), (6a), and (6b), assuming the following is true on Iapetus: $g = 23$ g/cm^2, $\delta = \rho = 1$ g/cm^3, $U = 4.5$ km/s, $D_{tr} = 15$ km (from Zahnle et al. (2003)), a divot (at impactor $d = 100$ km) corresponds to a crater diameter $D = 600$ km on Iapetus (to be compared with $D = 400$ km on Pluto). The peak in Fig. 7 at roughly $D = 400$ km could be the signature of the divot; note the factor of six (value of the contrast c in the "divoted" size distribution) between the average R-value of ≈ 0.04 for the 100 km $< D <$ 300 km basins and $R = 0.25$ for the $D \approx 400$ km basins in Fig. 7.

The minor discrepancy between the 600 km predicted crater diameter D corresponding to the divot on Iapetus and what appears to be the divot in Fig. 6 at $D = 400$ km would be eliminated if one adjusted the assumed impactor albedo used to compute the impactor diameter corresponding to the H_g-magnitude (Eq. 1) for which the divot is pegged. Creating a crater with $D = 400$ km on Iapetus requires an impactor with diameter $d \simeq 60$ km, while $D = 600$ km corresponds to $d \simeq 100$ km. Because constant flux $\propto p * d^2$, where p is the albedo, a decrease in the divot impactor diameter d by a factor of (100 km/60 km) = 1.7 requires an albedo increase by a factor of 2.9 in order to move the crater diameter corresponding to the divot from $D = 600$ km to $D = 400$ km in Fig. 7. This would require modifying our nominal $p = 0.05$ albedo to $\simeq 0.15$. Observations estimate TNO albedos range from $\simeq 2.5\%$ to $\simeq 25\%$ (Stansberry et al., 2008; Lacerda et al., 2014; Fraser et al., 2014) so a mean visual albedo of $p = 15\%$ may be reasonable. It is intriguing that one can use the basin excess on ancient cratered

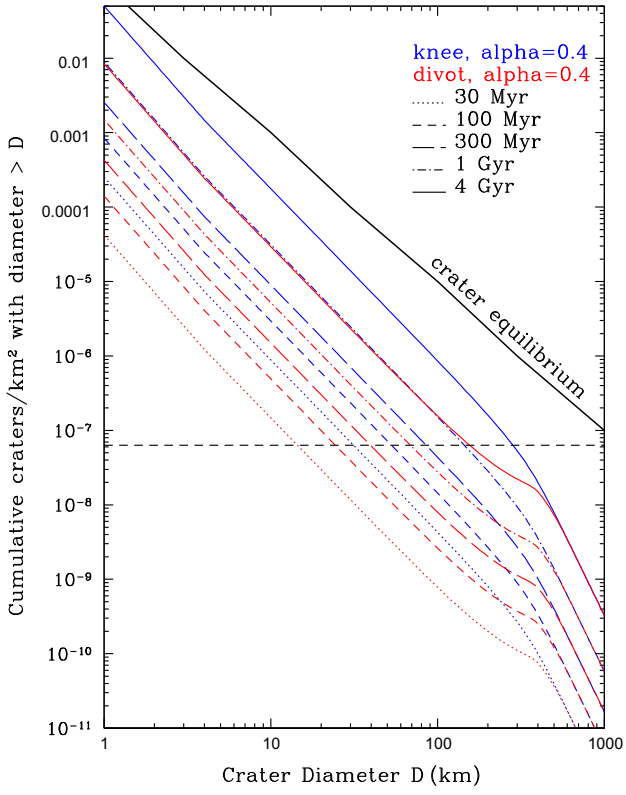

Fig. 5. Logarithm of crater density (# craters/km^2) larger than a given crater diameter D on Pluto's surface versus the logarithm of the crater diameter for an impactor size distribution with a knee and with a divot at various surface ages. The solid black line is the crater equilibrium curve from Melosh (1989), his Fig. 10.2, which is $R = 0.22$ or cumulative number $0.07N_s$ in his figure. The horizontal line at −7.2 corresponds to 1 crater/Pluto surface. The subtle change in slope at $D = 4$ km corresponds to the transition from simple to complex craters.

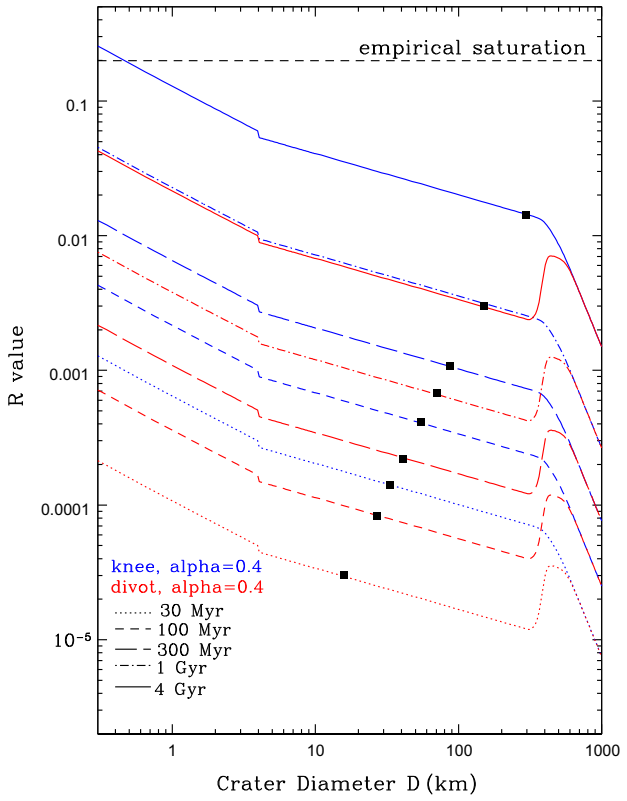

Fig. 6. Relative crater frequency plot of the same information in Fig. 5. The bump at $D \approx 400$ km is due to the divot. The black squares correspond to 1 crater/Pluto surface on a cumulative plot, so unfortunately nothing to the right of those dots will likely be visible on Pluto's post-installation terrains, except by statistical fluctuation. It would require many times the current integrated bombardment rate to bring this portion of the relative crater frequency to the visible range on Pluto. The sudden slope change at $D = 4$ km corresponds to the transition from simple to complex craters as shown in Fig. 5.

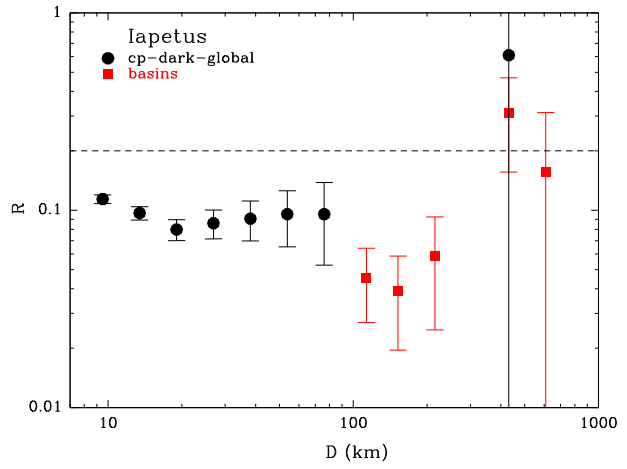

Fig. 7. Relative crater densities as determined by Kirchoff and Schenk (2010) for Iapetus, the second largest midsized moon of Saturn. Compare with Fig. 6. Cratered plains (cp) refer to broad counting regions. The horizontal line is empirical saturation. Note the factor of six (value of the contrast c in the "divoted" impactor size distribution) between the average R-value of ≈ 0.04 for the 100 km $< D <$ 300 km basins and $R = 0.25$ for the $D \approx 400$ km basins.

surfaces to find the physical impactor diameter corresponding to the divot, and therefore the albedo, given the uncertainty inherent in the crater scaling law. Because the uncertainties in the crater scaling law (Eqs. (5), (6a), and (6b)) outweigh the uncertainty in TNO albedo measurements, the albedo uncertainties are not important to the interpretations presented in this paper.

However, given that the scattering objects are the primary impacting population onto Iapetus one would not expect the "excess basin" feature to have arisen in the past 4 Gyr, but rather during the first 0.5 Gyr of Solar System evolution (sometimes referred to as the Late Heavy Bombardment (LHB), at least in regard to Saturn). Such a feature would be natural if the outer Solar System projectile population had a primordial divot at the break diameter of $d \sim 100$ km. In a plausible "born big" accretional scenario (discussed in Shankman et al. (2013) and Johansen et al. (2014)), the "smaller" $d < 100$ km projectiles could be extremely underabundant because they only exist as the collisional fragments of the $d > 100$ km bodies that are the result of planetesimal formation; the small bodies slowly rise in number during the subsequent collisional evolution (see Campo Bagatin and Benavidez (2012) and Benavidez et al. (2012) for an illustration).

If Pluto, or possibly Charon, preserves its ancient surface, we expect a similar pattern of a large-basin excess to have been created when Pluto was in its pre-installation location, where the crater production rate was much higher but typical impact speeds may have been even lower[6] than in the modern environment. How visible this basin excess signal will be on Pluto depends on whether crater saturation has been reached and whether even in a saturated state the signature can persist (although the Iapetus case implies it can). Because the general form of the production population can be retained even in the saturated state when large impacts dominate, as Chapman and McKinnon (1986) and Richardson (2009) both conclude, this "basin excess" should still be present in terrains even after specific chronological utility has been lost. Such a terrain would still indicate a roughly 4 Gyr crater retention age. Note that the crater distribution superposed on the basin and its ejecta blanket could potentially provide an individual basin's age.

3.3. Returning to crater retention ages for young surfaces

Even if a basin excess is observed on Pluto or Charon, it may simply provide evidence for the presence of a divot in the impactor size distribution. This would not alleviate all uncertainties in the crater retention ages for young surfaces, because a precise measure of the contrast is needed to tell us how the well-characterized impactor size distribution connects to $d < 100$ km impactors that produce the measurable crater densities on Pluto. If the observed $D < 100$ km crater production function slope has a value of $\alpha \simeq 0.4$ or greater, then one is in the regime in which the small craters will saturate first. Thus, we expect that it will be possible to assign model-dependent surface ages, either using the most-abundant (small) craters visible in unsaturated regions, or using the diameters above which the surface is not saturated if the smallest craters have reached saturation (this is standard for "steep" impactor populations). We remind the reader that referring to "shallow" and "steep" size distributions in the outer Solar System is different than for the inner Solar System. What we refer to as a "shallow" Kuiper belt population (with $\alpha_{faint} = 0.4$ and $q_{faint} = 3$) is actually on the steep end insofar as inner Solar System crater populations are concerned (e.g., Chapman and McKinnon (1986), although when represented on a R plot, $q = 3$ is actually neither shallow nor steep), thus populations with $\alpha \sim 0.8$ ($q \sim 5$) are much steeper than are ever discussed in inner Solar System cratering. To quantify this, Fig. 6 shows that an R value of ≈ 0.02 at $D = 1$ km corresponds to about 1 Gyr of

[6] Recall that typical encounter speeds (velocity at infinity) go as $v_\infty \approx v_{kep}\sqrt{e^2 + i^2}$ for small eccentricity e and inclination i allowing $v_\infty \ll 2$ km/s in a dynamically cold pre-installation phase, where $e < 0.01$ may be typical.

bombardment for a knee scenario, but ≈ 4 Gyr for a divot. Because this is not saturated (R value < 0.2), if these impactor distributions are valid, any surface region reset after Pluto's installation onto its current orbit should not be saturated (except possibly at sub-km scales or by secondary craters; see Section 3.5) and a model-dependent age could be provided. Conversely, assuming the small impactor size distribution extrapolation follows a single slope of $\alpha_{faint} = 0.4$, any saturated surface in $D \geqslant 1$ km craters necessarily dates to the pre-installation phase in which there is no absolute calibration of the bombardment rate; we would conclude that little can thus be said about such a region other than it must date to at least $\gtrsim 4$ Gyr ago.

3.4. The effect of varying α_{faint}

To cover a portion of the plausible range of values for the logarithmic slope at the small end ($d < 100$ km) of the impactor size distribution, we computed cratering rates for two additional single-slope extrapolation α_{faint} values: $\alpha_{faint} = 0.3$ ($q_{faint} = 2.5$) and $\alpha_{faint} = 0.5$ ($q_{faint} = 3.5$). Table 4 shows the total cratering rates for these two values of α_{faint} as well as a repeat of the last line of Table 2 where $\alpha_{faint} = 0.4$ ($q_{faint} = 3$). The SPL is absent in Table 4 because the SPL cratering rates do not change when α_{faint} is varied. $D \geqslant 400$ km craters correspond to roughly the impactor diameter at the break in the power-law size distribution, so the cratering rates at this threshold diameter are also unchanged as α_{faint} varies. As one moves to smaller diameters, the cratering rates for different slopes diverge, while the factor-of-six difference between the knee and divot scenarios is maintained for crater diameters corresponding to $d < 100$ km impactors.

Fig. 8 compares the 4 Gyr relative crater frequency curves from Fig. 6 with the $\alpha_{faint} = 0.3$ and $\alpha_{faint} = 0.5$ cases. The figure indicates saturation for $D \lesssim 20$ km and $D \lesssim 3$ km for the $\alpha_{faint} = 0.5$ knee and divot scenarios, respectively, in $\simeq 4$ Gyr of bombardment. Thus, a saturated surface in $D \sim 1$ km craters does *not* necessarily date to the pre-installation phase. This only further complicates the interpretation of Pluto's cratering record.

Because New Horizons should be able to observe craters down to 1–2 km in diameter on the encounter hemisphere, and down to 500 m in diameter in a high-resolution swath (Young et al., 2008; Moore et al., 2014), saturation in either $D \lesssim 20$ km craters or $D \lesssim 3$ km craters could be visible on $\leqslant 4$ Gyr terrains if $\alpha_{faint} = 0.5$. No saturation in $D \lesssim 20$ km craters would put an upper limit on the value of α_{faint} at $\leqslant 0.5$, for a heavily cratered terrain and if the impactor size distribution has a single-slope extrapolation in either the form of a knee or a divot at $d = 100$ km down to sub-km sizes. For $10 \leqslant D \leqslant 100$ km, the slope of the production function may be able to be measured. Again, the slope alone will not be sufficient to provide an absolute age.

Fig. 8 clearly indicates that $\alpha_{faint} \approx 0.35$ would produce a flat distribution on the R-plot (corresponding to $q_{faint} = 2.75$). Varying α_{faint} slightly changes the amount of basin excess visible in the divot scenario, but this will not be discernible. The $\alpha_{faint} = 0.3$ ($q_{faint} = 2.5$) curve shows a situation where a long-term bombardment would eventually saturate at the largest size craters before the smaller size craters, but in this case, even the smallest primary craters will be far below saturation in 4 Gyr of bombardment. For $\alpha_{faint} = 0.5$, craters with $D \leqslant 3$ km or $D \leqslant 20$ km would be saturated for the divot and knee scenarios, respectively. This would mean a more restricted visible crater diameter range (larger than saturation) would be usable for making inferences about the production population.

Collisional evolution of the Kuiper belt size distribution would also affect the crater production function observed on Pluto, however it would only be important if the size distribution has a very steep slope down to small diameters, causing the abundant population of small (sub-km) Kuiper belt objects to collisionally evolve over the past 4 Gyr. Because this is at the small end of the size distribution, it would only affect the crater production function in the few-km crater diameter regime. Such a scenario would cause the ages computed in our analysis for few km craters to be too long since collisional evolution would infer more little (sub-km) Kuiper belt objects existed in the past than are present in the population today. The few-km-diameter crater regime, however, reaches into the population of secondary craters, which is not a complication we include in our analysis. The collisional evolution of the Kuiper belt, thus does not largely affect our analysis of the crater production functions on Pluto.

3.5. Secondary craters

The discussion has so far concentrated on primary craters. Secondary craters are expected on Pluto and Charon as well (Bierhaus and Dones, 2015), although of course they are generally much smaller than the primary craters that cause them. A general rule of thumb is that the largest secondaries are 0.05 the size of a given primary (Melosh, 1989), which is in line with more recent studies of icy satellite secondaries (Bierhaus et al., 2012; Singer et al., 2013). Although the largest, proximal secondaries on icy satellites can reach 0.1 the size of their generative primary, the sizes of distant secondaries, which are the ones that can be confused with the primary population (McEwen and Bierhaus, 2006), are much smaller. Secondary populations are generally quite "steep", with differential size–frequency indices (akin to q_{slope} for the impactor populations) > 3. Thus, steep crater SFDs on Pluto or Charon at sizes of a few km or less (Bierhaus and Dones, 2015) should be interpreted cautiously. This will depend on the characteristics of the global crater population, however; if there are relatively few large craters or basins, then their influence on the small crater population *that New Horizons can resolve* will be negligible. In addition, it is unclear if all characteristics of secondary crater production hold for the sub-hypervelocity impact regime. New Horizons should be able to find out, however. The exchange of ejecta between Pluto, Charon, and the four smaller satellites is possible (Stern, 2009). However, the resulting sesquinary craters produced by this exchange will be difficult to distinguish from secondary craters on Pluto.

3.6. Implications of a "wavy" size distribution

The above analysis has been performed assuming a single-slope extrapolation from $d > 100$ km impactors to smaller sizes. More likely, the break in the size distribution at $d = 100$ km is instead the first of several slope changes between the $d > 100$ km impactors and the sub-km regime as the "wavy" size distributions of the asteroid belt show. Proposals for outer Solar System populations were made by Minton et al. (2012) (hereafter referred to as M12) and Schlichting et al. (2013) (hereafter referred to as S13). S13's model for the collision-generated population of KBOs today (shown in their Fig. 7) has $\alpha_{bright} = 0.6$ ($q_{bright} = 4$) for $d > 60$ km, $\alpha_{faint1} = 0.2$ ($q_{faint1} = 2$) for 20 km $< d < 60$ km, $\alpha_{faint2} = 0.96$ ($q_{faint2} = 5.8$) for 2 km $< d < 20$ km, $\alpha_{faint3} = 0.32$ ($q_{faint3} = 2.6$) for 0.2 km $< d < 2$ km, and $\alpha_{faint4} = 0.54$ ($q_{faint4} = 3.7$) for 0.02 km $< d < 0.2$ km. S13 state the only difference between their small KBO size distribution and the results of the saturnian crater analysis of M12 (their Fig. 1) is that M12 find a shallower slope of $\alpha_{faint2} = 0.64$ ($q_{faint2} = 4.2$) for the 2 km $< d < 20$ km range. D. Minton (private communication, 2014) states M12 was preliminary, so we use his model as stated in Schlichting et al.

Table 4
Total *current* primary cratering rates onto Pluto for two impactor size distribution scenarios: a knee (top) and a "divot" (bottom) for 5 sample crater threshold diameters with three different values of logarithmic slope α_{faint}.

Logarithmic slope, α_{faint}	Current cratering rate $D \geqslant 400$ km (/yr) Knee/divot	Current cratering rate $D \geqslant 100$ km (/yr) Knee/divot	Current cratering rate $D \geqslant 30$ km (/yr) Knee/divot	Current cratering rate $D \geqslant 10$ km (/yr) Knee/divot	Current cratering rate $D \geqslant 3$ km (/yr) Knee/divot
0.3	6e−11 4e−11	1e−9 3e−10	1e−8 2e−9	8e−8 1e−8	7e−7 1e−7
0.4	6e−11 5e−11	3e−9 5e−10	4e−8 7e−9	5e−7 9e−8	9e−6 2e−6
0.5	6e−11 5e−11	5e−9 8e−10	2e−7 3e−8	4e−6 6e−7	1e−4 2e−5

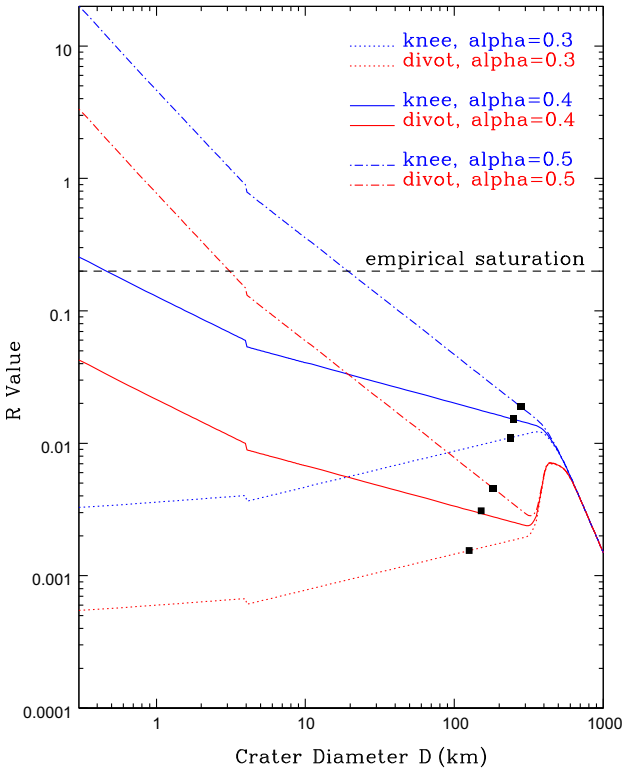

Fig. 8. Relative crater frequency plot, similar to Fig. 6, but for three values of α_{faint} over 4 Gyr of flux. The black squares correspond to 1 crater/Pluto surface on a cumulative plot, so unfortunately nothing to the right of those dots will likely be visible on Pluto's post-installation terrains, except by statistical fluctuation. The sudden slope change at $D = 4$ km corresponds to the transition from simple to complex craters.

(2013) simply as another illustrative example of a "wavy" size distribution.

Portions of this "waviness" below $d = 100$ km may already have been observed in the size distribution observations of the Jupiter family comets (JFCs) by Solontoi et al. (2012). Their Fig. 10 shows the cumulative number of JFCs as a function of radius assuming an albedo of $p = 0.04$. They find a break in the size distribution at $d \approx 6$ km from $\alpha = 0.73$ for $d \approx 6$–12 km to $\alpha = 0.2$ for $d \approx 2$–6 km. This break between the steep and shallow slopes does not quite match the location of the M12 and S13 models near $d = 2$ km where the latter models change from a steep slope ($\alpha_{faint2} = 0.96$ or $\alpha_{faint2} = 0.64$) to a shallower slope ($\alpha_{faint1} = 0.32$). However, repeating the albedo exercise of Section 3.2, an albedo $p = 0.24$ provides a factor of 3 decrease in break diameter (from $d = 6$ km to $d = 2$ km), which would shift the Solontoi et al. (2012) size distribution break to align with the similar diameter break in the M12 and S13 models at $d = 2$ km.

To illustrate how multiple slope changes in the KBO size distribution affects the cratering history of Pluto, we modeled the described size distributions of M12 and S13 by pegging these two size distributions to the CFEPS KBO sub-population estimates at $H_g = 9.0$ (corresponding to $d = 108$ km assuming an albedo of $p = 0.05$). Fig. 9 shows the cumulative crater density on Pluto using the M12 and S13 impactor size distributions. Because this is a cumulative plot, the abrupt slope transitions smooth out over a range of crater diameters. The smoothing effect is enhanced by our use of the realistic impact velocity spectrum. The two models lie on top of each other for $D \gtrsim 100$ km, then diverge due to their different slopes from 10 km $\lesssim D \lesssim 100$ km before becoming parallel for $D \lesssim 10$ km where their slopes once again match. The solid diagonal black line in Fig. 9, representing crater equilibrium, indicates the S13 impactor size distribution saturates for any $D \lesssim 20$ km in 4 Gyr, while the M12 model does not saturate for $D \geqslant 1$ km. The S13 model in fact saturates for $D \lesssim 12$ km craters in only ≈ 1 Gyr. To link this back to the discussion in Section 3.4, both the S13 and $\alpha_{faint} = 0.5$ size distribution models saturate for $D \lesssim 10$ km craters, so observing saturated craters at this diameter range in New Horizons images will not determine the preferred size distribution model alone. The *shape* of the production function may nonetheless be present in Pluto's cratering record for craters with 10 km $\lesssim D \lesssim 100$ km, however, as long as saturation of the entire surface in small craters does not corrupt (i.e., degrade recognition of) the $D = 10$–100 km range.

Fig. 10 compares the relative crater frequency for the M12 and S13 models with the single-slope knee and divot scenarios presented earlier, for three sample bombardment durations. The drop in relative crater frequency from $D \approx 400$ km and $D \approx 100$ km in Fig. 10 for the M12 and S13 models is due to their shallow slope ($\alpha_{faint1} = 0.2$) in this crater diameter range being less than $\alpha \approx 0.35$. [7] This drop is different from the sudden drop in the relative crater frequency from $D \approx 500$ km to $D \approx 350$ km due to a divot in the impactor size distribution. As shown in Fig. 10, the basin excess due to the divot is more tightly confined to a small crater diameter range than the broad "dip" that would be present from $D = 50$ km to $D = 500$ km in the M12 and S13 models. Unfortunately, this size range will not be expressed in the Pluto cratering record in 4 Gyr of bombardment (solid squares in Fig. 10, although it might be going further back in time). The very steep slope between $D = 10$ km and $D = 100$ km in the S13 model produces rapidly increasing crater densities as D drops and saturates at even $D \approx 20$ km in 4 Gyr. We also note the upturn (steepening) of the crater SFD at small ($D < 2$ km) sizes in Fig. 10. Nominally, this could be interpreted as

[7] For the crater scaling law in use, $\alpha \simeq 0.35$ produces an R value that does not depend on D.

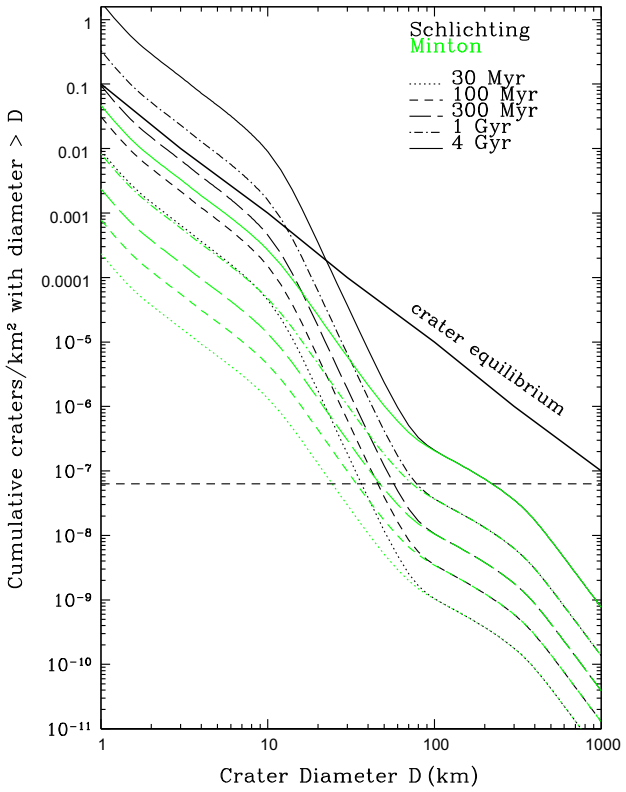

Fig. 9. Logarithm of crater density (# craters/km^2) larger than a given crater diameter D on Pluto's surface versus the logarithm of the crater diameter D for the impactor size distributions from Minton et al. (2012) and Schlichting et al. (2013), for various exposure durations. The solid black line is the crater equilibrium curve from Melosh (1989). The horizontal line at −7.2 corresponds to 1 crater/Pluto surface.

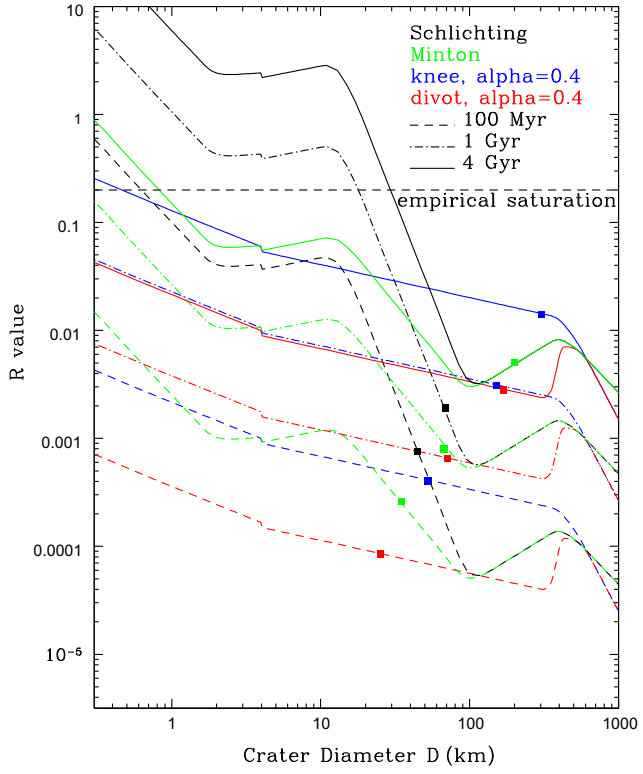

Fig. 10. Relative crater frequency plot for the Minton et al. (2012) and Schlichting et al. (2013) impactor size distribution models and the $\alpha_{faint} = 0.4$ knee and divot extrapolations. The colored squares correspond to 1 crater/Pluto surface on a cumulative plot, so nothing to the right of those dots will likely be visible on Pluto's post-installation terrains.

evidence of secondary contamination as discussed above, but given the overall steepness of the M12 and S13 distributions, this would be physically unlikely.

The crater diameter range most reliable for the interpretation of Pluto's cratering record provided by the New Horizons spacecraft will likely be the $D \approx 30$—100 km range where one might hope to have the slope of the production function measured. Because we expect models with multiple slope changes make a more realistic representation of the impactor size distribution than a single slope, the "waviness" should be present in the production function. The range for which the production function would be measurable obviously increases as a function of surface age (left of the colored squares in Fig. 10). While direct observation of the crater distribution in the 30 km $\leqslant D \leqslant$ 100 km range will thus establish relative numbers of impactors as well as the shape of the production function, it will *not* by itself provide a firm connection to the absolutely calibrated $d > 100$ km impactors. As a result, only model-dependent ages can be found for the surfaces of Pluto and Charon.

Even if the surface of Pluto (and especially Charon) is completely saturated, one would still hope to be able to find the largest "fresh" crater to have formed on the surface and attempt to measure the production function superposed on this "fresh" crater and its ejecta blanket. Using any of the size distributions discussed (S13 model, M12 model, knee with $\alpha_{faint} = 0.4$, or divot with $\alpha_{faint} = 0.4$), we compute that to 95% confidence there has been at least one $D \gtrsim 50$ km crater formed within the past 1 Gyr and this thus sets the scale for the largest "fresh" feature one might hope to find on Pluto's surface. Fig. 11 is similar to Fig. 9 for up to 1 Gyr of bombardment from the S13 and M12 models. The horizontal line corresponds to 1 crater/surface area of that largest "fresh" $D \gtrsim 50$ km crater and its ejecta blanket (which we take to be roughly 100 km in diameter). The superposed production function can thus be measured above this horizontal line.

Because the S13 and M12 models have the same slope for the portion of the impactor size distribution corresponding to the above crater diameter range, only model dependent ages can be determined for such a surface. Such ages will differ by a factor of ≈ 30 between the S13 and M12 models, as indicated by the near overlap of the 1 Gyr M12 curve and the 30 Myr S13 curve in Fig. 11. However, the two scenarios yield a rather different qualitative picture. The $D \gtrsim 50$ km crater floor that formed to 95% confidence ≈ 1 Gyr ago will already have saturated if the S13 model is correct (and, dramatically, due to all craters at *all* diameter bins below ≈ 15 km). Even at the mean formation interval[8] for a $D \gtrsim 50$ km crater of 300 Myr, the largest "fresh" crater floor present on Pluto should have nearly reached saturation in the S13 model scenario. Therefore, the S13 model would predict there are most likely *no* large unsaturated craters and corresponding ejecta blankets on Pluto; only such a steep size distribution can cause the surface to saturate so quickly. Observing such a situation on Pluto would support the occultation measurement (Schlichting et al., 2012) motivating the S13 model.

If, however, one or several un-saturated "fresh" $D \gtrsim 50$ km crater floors are present on Pluto, a superposed crater production function should be measurable (depending on proximity to the terminator at encounter), and a model-dependent age (varying by a factor of ≈ 30) could be assigned to the region. For example, again examine the overlapping 30 Myr S13 and 1 Gyr M12 model curves

[8] That is, the mean time between formation of $D \gtrsim 50$ km craters on Pluto is 300 Myr, even if it takes a Gyr to be 95% confident that one will be formed on the surface.

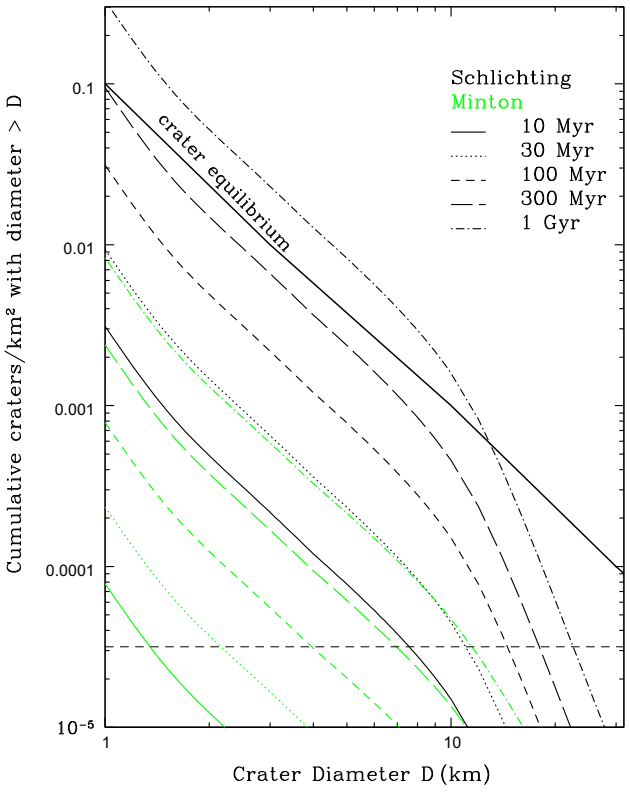

Fig. 11. Logarithm of crater density (# craters/km^2) larger than a given crater diameter D on Pluto's surface versus the logarithm of D, for the impactor size distribution from Minton et al. (2012) and Schlichting et al. (2013), for various exposure durations. The dashed horizontal line corresponds to one crater superposed on a $D \gtrsim 50$ km crater and its 100 km diameter ejecta blanket (to 95% confidence the largest "fresh" crater which will have formed in the past 1 Gyr). The solid diagonal line is the small-crater equilibrium curve. The S13 model indicates it is unlikely the ejecta blanket of any $D \gtrsim 50$ km "fresh" crater on Pluto's surface will not appear heavily cratered and near saturation (e.g., see the crater Penelope on Tethys). In contrast, the M12 model suggests the "freshest" $D \gtrsim 50$ km crater floor will not be near saturation and a production function should be measurable on the crater floor and surrounding ejecta blanket. A "freshest" $D \gtrsim 50$ km crater which is lightly cratered would need to be tens of Myr old in the S13 model scenario.

in Fig. 11. Nominally the production function might look like the 1 Gyr M12 model (with a largest superposed crater of $D \approx 12$ km); but the S13 model would imply a 30 Myr crater retention age and that the 50 km crater formed extremely recently. However, the S13 model suggests a mean formation interval of 300 Myr for $D \gtrsim 50$ km, with thus only a low 30/300 = 10% probability of the crater having formed recently enough to be so lightly cratered, making this proposed projectile size distribution less likely. In contrast, the M12 model would expect a mean formation interval of ≈ 1 Gyr for $D \gtrsim 50$ km craters. There is thus likely a way to test the qualitative difference between these two models from the New Horizons data alone at least in terms of likelihood.

This "largest fresh crater in a Gyr" argument was chosen to illustrate how quickly the very steep size distribution of the S13 model would predict even the "freshest" crater floors saturate. The largest "fresh" crater expected to form (95% confidence) can, however, be computed for any time interval. For an event in the last Gyr, neither model would predict the floor of the "fresh" crater to be saturated, however the number of craters expected to be on the crater floor and its ejecta blanket will be different between the two models as the reasoning above describes. For example, the largest "fresh" crater expected to form (to 95% confidence) in 100 Myr ($D \gtrsim 30$ km) is not much smaller than in 1 Gyr ($D \gtrsim 50$ km) due to the steep impactor size distribution in this portion of the crater production function. The S13 model would predict there should be a measurable production function on this surface, especially if the crater is close to 100 Myr old. The M12 model, on the other hand, would predict very few craters should be present on the "freshest" $D \gtrsim 30$ km crater if it formed 100 Myr ago. Qualitatively, the S13 model's very steep size distribution would predict that all "fresh" crater floors should be quickly recratered and the M12 model would predict recratering to occur less rapidly.

We note this line of argument will be complicated or obviated if Pluto's surface is extremely young due to surface-atmospheric interactions (Stern et al., 2015). An analogous argument may work for Charon, however, and is discussed in Section 3.7.

3.7. Charon

Zahnle et al. (2003) state that the impact rate onto Charon is 16% that on Pluto accounting for gravitational focusing with an average system encounter velocity of 1.9 km/s. Using our modified Öpik collision probability code, we find the total impact rate onto Charon from the various Kuiper belt sub-populations for $H_g < 9$ is 9.2×10^{-12}/yr ($\pm 50\%$ given the uncertainties in the $H_g < 9$ population estimates). This is $(9.2 \times 10^{-12}\text{/yr})/(4.8 \times 10^{-11}\text{/yr}) = 0.19$ that of the total impact rate on Pluto, in rough agreement with Zahnle et al. (2003). This multiplicative factor does not, however, convert total Pluto cratering rates into total Charon cratering rates. The crater scaling law (shown in Eqs. (5), (6a), and (6b)) for Charon is influenced by the different value of gravitational acceleration g on Charon ($g = 26$ cm/s^2) from on Pluto ($g = 64$ cm/s^2) and a different impact velocity range because Charon's escape speed ($v_{esc} = 0.675$ km/s) is smaller than Pluto's ($v_{esc} = 1.2$ km/s).[9] The difference in the crater scaling law between Pluto and Charon means each crater diameter corresponds to a different impactor diameter for Charon than on Pluto, so each size distribution extrapolation (SPL/knee/divot) produces a different cratering rate *larger than some fixed crater D* on Charon compared with that on Pluto. The outcome is shown in Table 5.

The cratering rates for fixed threshold crater diameter on Charon are $\approx 40\%$ that on Pluto for the SPL cases and $\approx 25\%$ for the knee and divot scenarios. It is unsurprising that the knee and divot scenarios give the same multiplicative factor for the cratering rate on Charon to that on Pluto, because they have the same slope for $d < 100$ km impactors. The SPL slope diverges from the knee/-divot slope at smaller diameters, so because Charon's cratering rate accesses smaller impactors than Pluto for the same crater diameter threshold, the Charon SPL cratering rates should be a larger percentage of the Pluto SPL cratering rates than for the Charon-to-Pluto knee/divot cratering rates. To turn the total cratering rates into the integrated number of craters estimated on Charon's surface over the last 4 Gyr, the cratering rates shown in Table 5 should be multiplied by an average EBF of 1.5 and 4 Gyr. For example, the integrated number of $D \geqslant 100$ km craters on Charon for the knee scenario is 7e-10 * 1.5 * 4e9 = 4 craters. Since there is not a simple conversion from cratering rates on Pluto to those on Charon, Fig. 12 provides both the crater density plot and R-plot for Charon using the single-slope knee/divot size distribution extrapolations with $\alpha_{faint} = 0.4$ as well as the M12 and S13 size distributions.

This allows model-dependent ages to be determined for a post-installation Charon just as is possible for a post-installation Pluto as discussed in Sections 3.1 and 3.3 above. As implied earlier, Pluto's active surface–atmosphere exchange and volatile surface

[9] For a typical v_∞, a fixed-diameter impactor is accelerated less by the smaller gravitational focusing of Charon compared with that of Pluto, but the ≈ 2.5 times smaller gravitational acceleration g for Charon outweighs this velocity effect, resulting in larger craters on Charon than on Pluto for a fixed impactor diameter.

Table 5
Current total primary cratering rates on Charon (≈ 25% to ≈ 40% those on Pluto) using our derived impact velocity distribution for all Kuiper belt sub-populations and three impactor size distribution scenarios: single power-law (SPL) (top), knee (middle), and "divot" (bottom) for 5 threshold crater diameters.

Size distribution extrapolation	Current total cratering rate $D \geqslant 400$ km (/yr)	Current total cratering rate $D \geqslant 100$ km (/yr)	Current total cratering rate $D \geqslant 30$ km (/yr)	Current total cratering rate $D \geqslant 10$ km (/yr)	Current total cratering rate $D \geqslant 3$ km (/yr)
SPL	2e−11	1e−8	4e−6	6e−4	2e−1
Knee	2e−11	7e−10	1e−8	1e−7	3e−6
Divot	1e−11	1e−10	2e−9	2e−8	4e−7

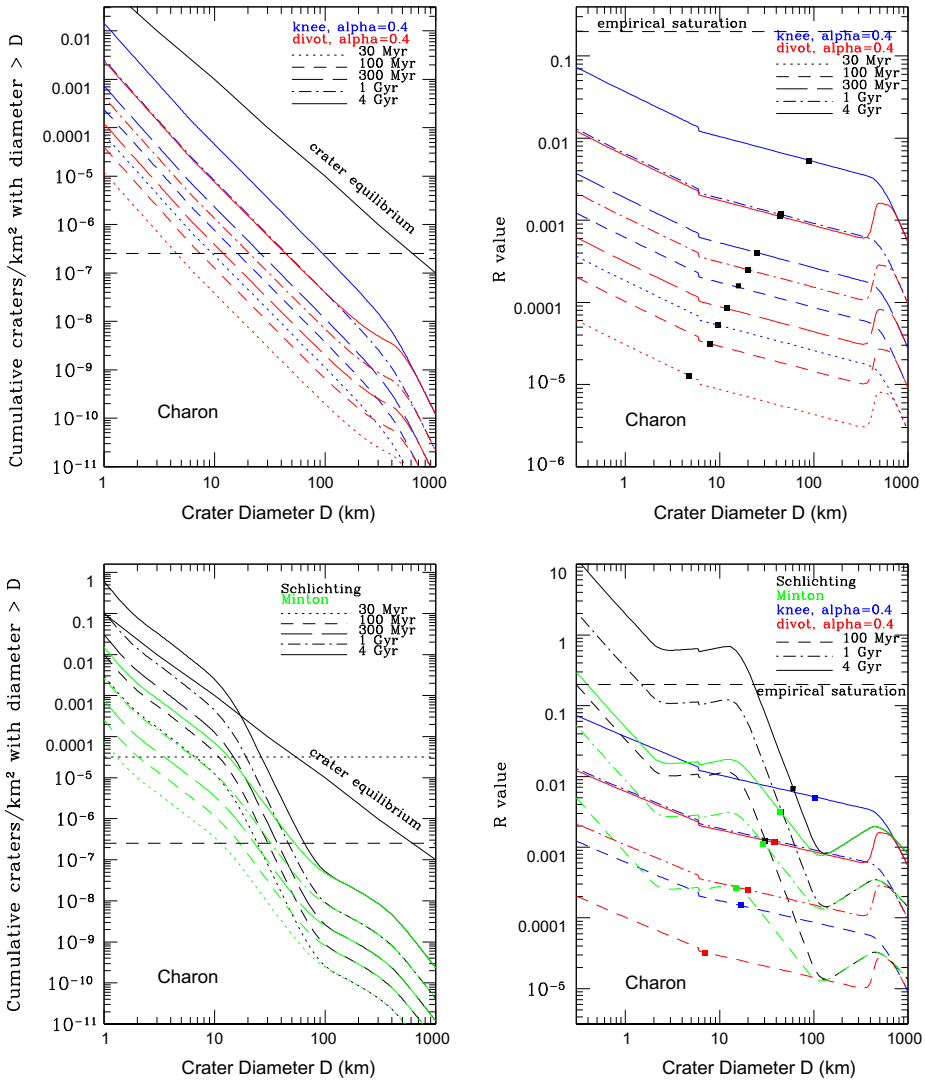

Fig. 12. Top left: similar to Fig. 5 except for Charon. The horizontal line at −6.6 corresponds to 1 crater/Charon surface. Top right: relative crater frequency plot for Charon. Similar to Fig. 6 except for Charon. Bottom left: similar to Fig. 9 except for Charon. Bottom right: similar to Fig. 10 except for Charon.

ices (CH_4, N_2) may work together to yield either a resurfaced young surface or to at least degrade topography on an older, heavily cratered surface (Stern et al., 2015). Charon, however, has none of these ices on its surface to our knowledge, no detectable atmosphere (Sicardy et al., 2006), and as a smaller body should be internally cooler and less active (McKinnon et al., 2008). It should possess older if not ancient surfaces. In principle, a basin excess due to the presence of a divot in the impactor differential size distribution (discussed in Section 3.2) may possibly be visible on Charon's most ancient surfaces. Note that the visible crater diameter range for which the production function (over 4 Gyr) can be measured is shifted to slightly smaller craters on Charon than on Pluto, in part, because Charon is a smaller body and cannot have basins approaching its own size. The crater SFDs measured on both bodies for these overlapping crater diameter ranges ($D = 20$—60 km on Charon and $D = 30$—100 km on Pluto) should provide the most reliable insights into the cratering history of the Pluto system and thus the size distributions in the Kuiper belt. Note that because Charon is tidally locked, a leading/trailing craterasymmetry is possible; the ratio $v_{orb}/v_{\infty} \sim 0.1$ is comparable to that of Earth's Moon Gallant et al., 2009 and so a ∼10% enhancement (deficit) of the of the crater density near Charon's apex (antapex) of motion relative to the mean crater density may be visible if the global coverage is sufficient.

To parallel the discussion at the end of Section 3.6, the largest "fresh" crater to have formed on Charon in 3 Gyr (chosen to illustrate the timescale the S13 model predicts rapid resaturation for Charon, compared with 1 Gyr on Pluto) to 95% confidence according to the S13 impactor size distribution model is, coincidentally, also ≈ 50 km in diameter. As shown in Fig. 11, the horizontal line at -4.5 in the bottom left panel of Fig. 12 corresponds to 1 crater/-surface area of that largest "fresh" $D \gtrsim 50$ km crater and its 100 km ejecta blanket. Just as on Pluto, the S13 model would predict this $D \gtrsim 50$ km crater should saturate quickly (though not as quickly as the analog on Pluto), whereas the M12 model would not predict this crater to reach saturation in 3 Gyr. No matter the size of the "freshest" crater one looks for on Charon (as on Pluto), the distinguishing property of the two size distribution models is how likely the crater is to be recratered after formation.

3.8. The four smaller moons

We have not repeated our full analysis for the four smaller satellites of Pluto (Styx, Nix, Kerberos, and Hydra). Instead, we have estimated the time (to roughly a factor of three accuracy) it would take for each of these satellites to be catastrophically disrupted using the current Kuiper belt sub-populations. Our estimate is based on the timescale between collisions for catastrophic dispersal of the target body, calling this the "disruption timescale". We compute one disruption timescale estimate for Nix and Hydra since they are of comparable size and another for Styx and Kerberos. Taking the diameter of Nix and Hydra to be ≈ 45 km (using mass, albedo = 0.4, and density estimates from Kenyon and Bromley (2014)), we use the catastrophic disruption threshold equation for the dispersal of half the target mass from Leinhardt and Stewart (2012),

$$Q^*_{RD} = 0.5\mu V^{*2}/M_{total} \tag{8}$$

where Q^*_{RD} is the specific energy required for dispersal of a catastrophically disrupted body, μ is the reduced mass ($M_{projectile}M_{target}/M_{total}$), V^* is the critical impact velocity for catastrophic disruption, and M_{total} is the total mass of the projectile and target. Assuming $M_{target} \gg M_{projectile}$, we solve the above equation for the mass of the projectile needed to disperse the target, assuming $V^* \approx 1.5$ km/s (mostly from v_∞ since the orbital speed around the Pluto–Charon barycenter and escape velocity are small) and estimating Q^*_{RD} from Fig. 11 of Leinhardt and Stewart (2009) for an icy target 45 km in diameter ($Q^*_{RD} = 7 \times 10^3$ J/kg, similar to that from Fig. 7 of Benz and Asphaug (1999)). We find that for catastrophic dispersal of either Nix or Hydra an impactor with diameter $d \geqslant 8$ km is needed.[10] Scaling the impact probability onto Pluto by the ratio of surface areas corrected for gravitational focusing gives the impact probability (/yr/projectile) for each sub-population onto Nix and Hydra. Multiplying each impact probability by the number of objects with $d \geqslant 8$ km for each sub-population gives the catastrophic disruption rate (/yr) for each sub-population. The resulting total current catastrophic disruption rate onto Nix and Hydra is 3.5×10^{-12}/yr for the $\alpha_{faint} = 0.4$ knee size distribution scenario. The disruption time for Nix and Hydra is therefore ≈ 300 Gyr for the $\alpha_{faint} = 0.4$ knee size distribution extrapolation for the *current* impactor population, and six times this, ≈ 1800 Gyr, for the divot. Integrating back to the larger impact rate $\simeq 4$ Gyr ago, the disruption time decreases to ≈ 200 Gyr for the knee scenario and ≈ 1200 Gyr for the divot. Comparing these estimates with those from the two "wavy" impactor size distributions, at this impactor size, the number of objects in the projectile population is similar to the knee scenario, so these "wavy" size distributions also would not result in catastrophic disruption of Nix and Hydra. Even if the critical impact velocity is increased to the tail of Pluto's impact velocity spectrum (6 km/s), where the speeds are higher but the impact probabilities are lower, the disruption timescale under the current bombardment is still longer than the age of the Solar System.

A similar argument was followed for Styx and Kerberos with diameters of roughly 10 km (mass and density estimates from Kenyon and Bromley (2014)), where we estimate Q^*_{RD} for an icy target 10 km in diameter ($Q^*_{RD} = 8 \times 10^2$ J/kg). Using the same reasoning as before, the current disruption timescale for Styx and Kerberos is therefore ≈ 70 Gyr for the $\alpha_{faint} = 0.4$ knee size distribution extrapolation under the current impactor population estimates, and six times this, ≈ 420 Gyr for the divot. Again, no scenarios result in Styx and Kerberos being catastrophically disrupted in the past ≈ 4 Gyr.

This begs the question of the smallest satellite that could survive against catastrophic disruption in the current bombardment environment. Fig. 13 shows the catastrophic disruption timescale (in Gyr) as a function of target radius (in m) for the Q^*_{RD} curves from Leinhardt and Stewart (2009) and Benz and Asphaug (1999). The Benz and Asphaug (1999) curve for impacts at 3 km/s and an incidence angle of 45° is most typical for impacts in the Kuiper belt, so we will use it in the discussion to follow, while the Leinhardt and Stewart (2009) curve for low speed, head-on collisions is shown for comparison. As can be seen in Fig. 13, for a knee size distribution with $\alpha_{faint} < 0.5$ (down to sub-km sizes) all target sizes would survive catastrophic disruption over the past 4 Gyr. As the target size decreases, the $\alpha_{faint} = 0.4$ knee size distribution corresponds to a situation where the cumulative number of impactors available to catastrophically disrupt the target increases at the same rate that the surface area of the target decreases (both as d^2), causing the two effects to cancel. This results in the catastrophic disruption rate decreasing as large targets get smaller (down to $d = 100$ m) and then increasing at smaller sizes as targets enter the strength-scaled regime for Q^*_{RD}. As α_{faint} decreases, the catastrophic

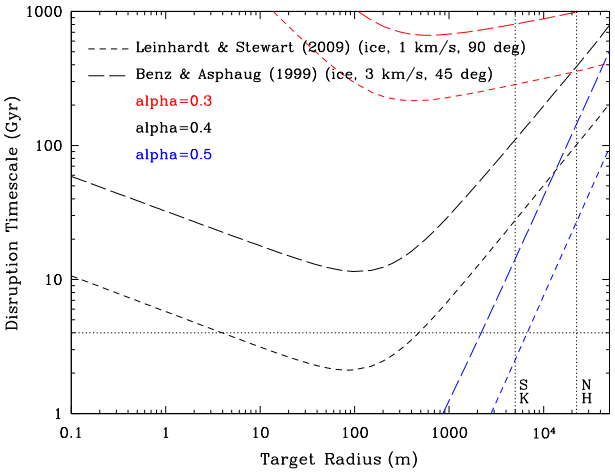

Fig. 13. Catastrophic disruption timescale (Gyr) as a function of target radius (m) for the Q^*_{RD} curves from Leinhardt and Stewart (2009) and Benz and Asphaug (1999) and three values of α_{faint} (size distribution with a knee). The vertical line at $r = 5$ km is roughly the radius of Styx and Kerberos and the vertical line at $r = 22.5$ km is roughly the radius of Nix and Hydra. For 3 km/s impacts at an incidence angle of 45° and $\alpha_{faint} = 0.4$, all size targets are able to survive against catastrophic disruption in the past 4 Gyr. For $\alpha_{faint} = 0.4$, the catastrophic disruption timescales for Styx and Kerberos is ≈ 100 Gyr and ≈ 400 Gyr for Nix and Hydra.

[10] Strictly speaking, these estimates are for disassembly of the moon against its own gravitational binding. The dispersed fragments would mostly remain in orbit around Pluto–Charon and reassemble. Even larger impactors would be necessary to disperse a small moon permanently (eject fragments onto heliocentric orbits).

disruption timescale moves to higher values as the cumulative number of impactors rises less steeply at small sizes, resulting in longer timescales between catastrophic disruption events. Conversely, as α_{faint} increases and more small impactors are available, the catastrophic disruption timescale drops. For $\alpha_{faint} = 0.5$ and typical impacts in the Kuiper belt, the Benz and Asphaug (1999) curve shows that the smallest target expected to survive catastrophic disruption in the last 4 Gyr is ≈ 4 km in diameter. Thus, if New Horizons finds satellites in the Pluto system that are smaller than ≈ 4 km in diameter, it either means an impactor size distribution with $\alpha_{faint} \geqslant 0.5$ (down to sub-km sizes) can be ruled out or that those satellites have catastrophically disrupted and reassembled in the past 4 Gyr. In principle, one could use the slope of the crater production function (for the sub-km diameter range) on Pluto or Charon to determine which of these two scenarios is more likely to be true.

Returning to the Pluto system four small satellites, Fig. 13 shows that for typical impacts in the Kuiper belt (given by the Benz and Asphaug (1999) curve) it is unlikely that any of the four small satellites have catastrophically disrupted and reassembled in the past 4 Gyr.

4. Summary and conclusions

By combining the contributions of each Kuiper belt sub-population from the well-calibrated CFEPS (Petit et al., 2011; Gladman et al., 2012) model and the KRQ11 (Kaib et al. 2011) scattering object model calibrated by Shankman et al. (2013), the impact rates and especially impact velocity spectra onto Pluto as presented here are currently state of the art. Pluto's environment before its installation onto its current orbit (which occurred at least 4 Gyr ago) is unknown, so primary cratering rates have been presented for "current day" timescales (a few hundred million years) and the number of craters larger than a threshold diameter D have been provided for Pluto's post-installation phase covering the past $\simeq 4$ Gyr of the Solar System's history accounting for the natural decay of each Kuiper belt sub-population. We find it is unlikely Pluto has been hit by even a single impactor that would create a $D > 400$ km crater, eliminating the chance that Pluto's post-installation cratering record can be immediately linked to the absolutely-calibrated impactor size distribution for $d > 100$ km. As a result, in order to date the surfaces of Pluto and Charon using observed crater densities, assumptions must be made about how the impactor size distribution extrapolates to small (sub-km) sizes. This is fraught with uncertainty, since we do not know how to connect the $d > 100$ km impactors to the smaller impactors. In this study we first adopt a single-slope $\alpha_{faint} = 0.4$ ($q_{faint} = 3$) power-law for the faint end ($d < 100$ km) of the size distribution, which is motivated by direct observations of small scattering objects, and highlight the factor-of-six variation between the knee and "divot" size distribution scenarios for this size regime. In addition, we show the effect of varying α_{faint} (to $\alpha_{faint} = 0.3$ and $\alpha_{faint} = 0.5$) on Pluto's cratering record. We also study how the "wavy" size distributions of Schlichting et al. (2013) and Minton et al. (2012) (as presented in Schlichting et al. (2013)), which include several slope changes between the $d = 100$ km impactors and the sub-km regime, would manifest in Pluto's cratering record.

Complications and Insights into computing and interpreting New Horizons observations of the cratering record on Pluto and its satellites include:

- No single Kuiper belt sub-population contributes the majority of the impact flux on the surface of Pluto (in fact, four sub-populations dominate the impact flux: the $q < 42$ AU hot classical mains, the $q < 42$ AU stirred classical mains, the classical outers, and the plutinos, each providing roughly equal contributions), so multiple Kuiper belt sub-populations must be used to accurately determine cratering rates. It is important to note that Pluto is impacted by a wider variety of Kuiper belt sub-populations than the satellites of the giant planets, particularly by the cold classical objects, which do not reach the giant planet region.
- Impact velocities onto Pluto range from 1.2 km/s (Pluto's escape speed) out to a tail at ≈ 6 km/s, so more smaller impactors can be accessed when computing the cratering rates on Pluto than a simple-impact-velocity assumption would give, resulting in slightly higher cratering rates than previously estimated, which translates into younger surface ages.
- The production function present in Pluto's cratering record will not link the absolutely calibrated impactor size distribution for $d > 100$ km objects to the size distribution of the $d < 100$ km impactors, because we do not expect craters created by the $d > 100$ km impactor size range to be present on Pluto's post-installation terrains.
- The result is that for any surface region reset after Pluto's installation onto its current orbit that has not reached saturation, absolute surface ages computed for Pluto and Charon simply cannot be done to better than the uncertainties in the impactor size distribution extrapolation. Thus, the best that can currently be done is to compute model-dependent ages for young surfaces on Pluto and Charon.
- If a divot is present in the impactor size distribution, a narrow-diameter-range "basin excess", similar to what has been observed on Iapetus, could possibly be visible on Pluto (or Charon) if a > 4 Gyr Pluto (or Charon) surface can be identified, implying that any basins found on Pluto must date back to Pluto's pre-installation phase.
- Because a size distribution model with multiple slope changes is likely a more accurate representation of the impactor population than an extrapolation of a single slope from impactors with $d = 100$ km down to sub-km sizes, the "waviness" may be easily discernible in Pluto's cratering record, both in the shape of the crater size distribution as well as in the crater saturation diameter, if non-saturated regions can be found.
- The "waviness" of the production function will most likely be discernable in the $D \approx 30$–100 km craters on Pluto and the $D \approx 20$–60 km craters on (smaller) Charon, making these the most reliable crater diameter ranges to the interpretation of the Pluto system cratering record provided by the New Horizons spacecraft. (These upper limits reflect likely maximum sized craters formed over 4 Gyr.)
- Even if the surface of Pluto appears saturated, one would like to measure the crater densities present on the largest "fresh" surfaces available. We estimate in Section 3.6 (at 95% confidence) that in 1 Gyr of bombardment at least one $D \gtrsim 50$ km crater will be created on Pluto (using any of the impactor size distribution models discussed, except the SPL), providing a fresh surface upon which the production function should be measurable. The M12 and S13 "wavy" impactor size distribution models would make different predictions about how likely that "fresh" $D \gtrsim 50$ km crater would be at or near saturation. Thus, there is likely a way to test the qualitative difference between these two models from the New Horizons data alone.
- We find that Charon's impact rate is 19% ($\pm 50\%$ uncertainty) that on Pluto, roughly consistent with Zahnle et al. (2003)'s estimate. However, because the cratering rate depends on the size distribution extrapolation used, Charon's cratering rate at fixed crater size is ≈ 25–40% that on Pluto for the knee/divot and SPL extrapolations, respectively.

- We estimate the timescale between collisions for catastrophic disruption for Pluto's four smaller moons (Styx, Nix, Kerberos, and Hydra). We find it is likely that none of these satellites have been catastrophically disrupted in the past ≈ 4 Gyr.
- For a knee size distribution with $\alpha_{faint} \leqslant 0.4$ (down to sub-km diameters), satellites of all sizes can survive catastrophic disruption in the past 4 Gyr. For $\alpha_{faint} \geqslant 0.5$ and typical Kuiper belt impact speeds, the smallest satellite that should survive catastrophic disruption in the past 4 Gyr is ≈ 4 km in diameter.
- It will be difficult to accurately interpret Pluto's cratering record until future observations of outer Solar System small bodies carefully probe the $d = 10$—100 km ($H_g = 9$—14) impactor size range (connecting the $d \approx 1$—10 km JFC size distribution (Solontoi et al., 2012) to the $d > 100$ km size distribution of the KBO/scattering/plutino populations from CFEPS (Petit et al., 2011; Gladman et al., 2012)) that could directly establish the linkage via the number distribution of the current projectile population. While there currently are thus fragments of the observed impactor size distributions across the outer Solar System small body populations, the entire diameter range is needed to make definitive statements about crater retention ages on the surfaces of Pluto and its moons.

5. Some predictions for the 2015 New Horizons observations of the cratering record in the Pluto system

- Craters large enough to connect Pluto's visible cratering record ($D < 100$ km) with the absolutely calibrated impactor size distribution for $d > 100$ km impactors will not be present on Pluto's post-installation terrains. The question will be how to separate Pluto's post-installation terrains from its pre-installation surfaces.
- A basin excess on pre-installation terrains due to the presence of a divot in the impactor size distribution may possibly be visible on Pluto (or Charon), similar to what has been observed on Iapetus. The extensive presence of volatile ices on Pluto may very well cause Charon to have an older surface than Pluto, in which case a basin excess could possibly only be visible on Charon.
- The impactor size distribution should be easily discernible in Pluto's cratering record via the shape of the production function in the $D \approx 1$—100 km range for craters larger than the saturation diameter (if any).
- Only the very steepest size distribution of Schlichting et al. (2013) would predict the cumulative crater density measured on Pluto or Charon should rise ≈ 4.5 orders of magnitude from the $D = 100$ km craters to the $D = 10$ km craters, implying rapid saturation of the surface, unlike the M12, knee, and divot size distribution models. Thus, we expect at least one "fresh" $D \approx 50$ km crater to exist on Charon that most likely has an unsaturated floor and ejecta blanket, which has been formed in the last 3 Gyr.
- If New Horizons finds satellites in the Pluto system smaller than ≈ 4 km in diameter, one could, in principle, use the slope of the crater production function (for the few-km diameter range) on Pluto or Charon to determine whether an impactor size distribution with $\alpha_{faint} \geqslant 0.5$ (down to sub-km sizes) can be ruled out or that those satellites have catastrophically disrupted and reassembled in the past 4 Gyr.

Acknowledgments

S. Greenstreet and B. Gladman acknowledge support from NSERC and CSA. W.B. McKinnon thanks the New Horizons project for support. We thank Luke Dones and Clark Chapman for their helpful reviews that greatly improved this paper.

References

Adams, E.R. et al., 2014. De-biased populations of Kuiper belt objects from the Deep Ecliptic Survey. Astron. J. 148, 55–71.
Alexandersen, M. et al., 2014. A carefully characterised and tracked trans-neptunian survey, the size-distribution of the plutinos and the number of neptunian trojans. arXiv: 1411.7953, 1–56.
Benavidez, P.G. et al., 2012. A comparison between rubble-pile and monolithic targets in impact simulations: Application to asteroid satellites and family size distributions. Icarus 219, 57–76.
Benz, W., Asphaug, E., 1999. Catastrophic disruptions revisited. Icarus 142, 5–20.
Bernstein, G.M. et al., 2004. The size distribution of trans-neptunian bodies. Astron. J. 128, 1364–1390.
Bernstein, G.M. et al., 2006. Erratum: "The size distribution of trans-neptunian bodies". Astron. J. 131 (2364).
Bierhaus, E.B., Dones, L., 2015. Craters and ejecta on Pluto and Charon: Anticipated results from the New Horizons flyby. Icarus 246, 165–182.
Bierhaus, E.B. et al., 2012. The role of ejecta in the small crater populations on the mid-sized saturnian satellites. Icarus 218, 602–621.
Campo Bagatin, A., Benavidez, P.G., 2012. Collisional evolution of trans-neptunian object populations in a Nice model environment. Mon. Not. R. Astron. Soc. 423, 1254–1266.
Chapman, C.R., McKinnon, W.B., 1986. Cratering of planetary satellites. In: Burns, J.A., Matthews, M.S. (Eds.), Satellites. University of Arizona Press, pp. 492–580.
Arvidson, R.E. et al., 1979. Standard techniques for presentation and analysis of crater size–frequency data. Icarus 37, 467–474.
de Elía, G.C., Di Sisto, R.P., Brunini, A., 2010. Impactor flux and cratering on the Pluto–Charon system. Astron. Astrophys. 521, A23.
Dell'Oro, A. et al., 2013. Statistics of encounters in the trans-neptunian region. Astron. Astrophys. 558, A95–A102.
Dones, L. et al., 1999. Dynamical lifetimes and final fates of small bodies: Orbit integrations vs Öpik calculations. Icarus 142, 509–524.
Dones, L. et al., 2004. Oort Cloud formation and dynamics. In: Festou, M.C., Keller, H.U., Weaver, H.A. (Eds.), Comets II. University of Arizona Press, pp. 153–174.
Dones, L. et al., 2009. Icy satellites of Saturn: Impact cratering and age determination. In: Dougherty, M.K., Esposito, L.W., Krimigis, S.M. (Eds.), Saturn from Cassini–Huygens. Springer Science Business Media B.V., pp. 613–635.
Doressoundiram, A. et al., 2008. Color properties and trends of the transneptunian objects. In: Barucci, M.A. et al. (Eds.), The Solar System Beyond Neptune. University of Arizona Press, pp. 91–104.
Duncan, M.J., Levison, H.F., 1997. A scattered comet disk and the origin of Jupiter family comets. Science 276, 1670–1672.
Durda, D.D., Stern, S.A., 2000. Collision rates in the present-day Kuiper belt and Centaur regions: Applications to surface activation and modification on comets, Kuiper belt objects, Centaurs, and Pluto–Charon. Icarus 145, 220–229.
Fraser, W.C., Kavelaars, J.J., 2008. A derivation of the luminosity function of the Kuiper belt from a broken power-law size distribution. Icarus 198, 452–458.
Fraser, W.C. et al., 2014. The absolute magnitude distribution of Kuiper belt objects. Astrophys. J. 782, 100–113.
Fuentes, C.I., Holman, M.J., 2008. A SUBARU archival search for faint trans-neptunian objects. Astron. J. 136, 83–97.
Gallant, J. et al., 2009. Current bombardment of the Earth–Moon system: Emphasis on cratering asymmetries. Icarus 202, 371–382.
Gladman, B. et al., 2001. The structure of the Kuiper belt: Size distribution and radial extent. Astron. J. 122, 1051–1066.
Gladman, B., Marsden, B.G., Vanlaerhoven, C., 2008. Nomenclature in the outer Solar System. In: Barucci, M.A. et al. (Eds.), The Solar System Beyond Neptune. University of Arizona Press, pp. 43–57.
Gladman, B. et al., 2012. The resonant trans-neptunian populations. Astron. J. 144, 23–47.
Gomes, R., 2003. The origin of the Kuiper belt high-inclination population. Icarus 161, 404–418.
Hahn, J.M., Malhotra, R., 1999. Orbital evolution of planets embedded in a planetesimal disk. Astron. J. 117, 3041–3053.
Hahn, J., Malhotra, R., 2005. Neptune's migration into a stirred-up Kuiper belt: A detailed comparison of simulations to observations. Astron. J. 130, 2392–2414.
Housen, K.R., Holsapple, K.A., 2011. Ejecta from impact craters. Icarus 211, 856–875.
Jewitt, D., Luu, J., Trujillo, C., 1998. Large Kuiper belt objects: The Mauna Kea 8K CCD Survey. Astron. J. 115, 2125–2135.
Johansen, A. et al., 2014. The multifaceted planetesimal formation process. In: Beuther, H. et al. (Eds.), Protostars and Planets VI. University of Arizona Press, pp. 547–570.
Kaib, N., Roškar, R., Quinn, T., 2011. Sedna and the Oort Cloud around a migrating Sun. Icarus 215, 491–507.
Kenyon, S.J., Bromley, B.C., 2014. The formation of Pluto's low-mass satellites. Astron. J. 147, 8–24.
Kirchoff, M.R., Schenk, P., 2010. Impact cratering records of the mid-sized, icy saturnian satellites. Icarus 206, 485–497.
Kozai, Y., 1962. Secular perturbations of asteroids with high inclination and eccentricity. Astron. J. 67, 591–598.
Kuchner, M.J., Brown, M.E., Holman, M., 2002. Long-term dynamics and the orbital inclinations of the classical Kuiper belt objects. Astron. J. 124, 1221–1230.
Lacerda, P. et al., 2014. The albedo-color diversity of transneptunian objects. Astron. J. Lett. 793, L2–L7.

Larsen, J.A. et al., 2001. The spacewatch wide-area survey for bright Centaurs and trans-neptunian objects. Astron. J. 121, 562–579.
Leinhardt, Z.M., Stewart, S.T., 2009. Full numerical simulations of catastrophic small body collisions. Icarus 199, 542–559.
Leinhardt, Z.M., Stewart, S.T., 2012. Collisions between gravity-dominated Bodies. I. Outcome regimes and scaling laws. Astrophys. J. 745, 79–105.
Levison, H.F., Duncan, M.J., 1997. From the Kuiper belt to Jupiter-family comets: The spatial distribution of ecliptic comets. Icarus 127, 13–32.
Levison, H.F. et al., 2008. Origin of the structure of the Kuiper belt during a dynamical instability in the orbits of Uranus and Neptune. Icarus 196, 258–273.
Lupo, M.J., Lewis, J.S., 1980. Mass-radius relationships and constraints on the composition of Pluto. Icarus 42, 29–34.
Lykawka, P.S., Mukai, T., 2005. Long term dynamical evolution and classification of classical TNOs. Earth Moon Planets 97, 107–126.
Malhotra, R., 1993. The origin of Pluto's peculiar orbit. Nature 365, 819–821.
Malhotra, R., 1995. The origin of Pluto's orbit: Implications for the Solar System beyond Neptune. Astron. J. 110, 420–429.
McEwen, A.S., Bierhaus, E.B., 2006. The importance of secondary cratering to age constraints on planetary surfaces. Annu. Rev. Earth Planet. Sci. 34, 535–567.
McKinnon, W.B., Schenk, P.M., 1995. Estimates of comet fragment masses from impact crater chains on Callisto and Ganymede. Geophys. Res. Lett. 22, 1829–1832.
McKinnon, W.B., Singer, K.N., 2010. Small impact craters on Triton: Evidence for a turn-up in the size–frequency distribution of small (sub-km) KBOs, and arguments against a planetocentric origin. Bull. Am. Astron. Soc. 42, 984.
McKinnon, W.B. et al., 2008. Structure and evolution of Kuiper belt objects and dwarf planets. In: Barucci, M.A. et al. (Eds.), The Solar System Beyond Neptune. University of Arizona Press, pp. 213–241.
Melosh, H.J., 1989. Impact Cratering: A Geologic Process. Oxford University Press, New York.
Minton, D.A. et al., 2012. Combining saturnian craters and Kuiper belt observations to build an outer Solar System impactor size–frequency distribution. Asteroids Comets Meteors Conf. 1667, 6348.
Moore, J.M. et al., 2014. Geology before Pluto: Pre-encounter considerations. Icarus 246, 65–81.
Morbidelli, A., 1997. Chaotic diffusion and the origin of comets from the 2/3 resonance in the Kuiper belt. Icarus 127, 1–12.
Nesvorný, D., Roig, F., Ferraz-Mello, S., 2000. Close approaches of trans-neptunian objects to Pluto have left observable signatures on their orbital distribution. Astron. J. 119, 953–969.
O'Brien, D.P., Sykes, M.V., 2011. The origin and evolution of the asteroid belt-implications for Vesta and Ceres. Space Sci. Rev. 163, 41–61.
Petit, J.M. et al., 2011. The Canada-France Ecliptic Plane Survey – Full data release: The orbital structure of the Kuiper belt. Astron. J. 142, 131–155.
Pokorný, P., Vokrouhlický, D., 2013. Öpik-type collision probability for high-inclination orbits: Targets on eccentric orbits. Icarus 226, 682–693.
Richardson, J.E., 2009. Cratering saturation and equilibrium: A new model looks at an old problem. Icarus 204, 697–715.
Schenk, P.M., Zahnle, K., 2007. On the negligible surface age of Triton. Icarus 192, 135–149.
Schlichting, H.E. et al., 2012. Measuring the abundance of sub-kilometer-sized Kuiper belt objects using stellar occultations. Astrophys. J. 761, 150–160.
Schlichting, H.E., Fuentes, C.I., Trilling, D.E., 2013. Initial planetesimal sizes and the size distribution of small Kuiper belt objects. Astron. J. 146, 36–42.
Schmidt, R.M., 1980. Meteor crater: Energy of formation – Implications of centrifuge scaling. Lunar Planet. Sci. 2099–2128.
Shankman, C. et al., 2013. A possible divot in the size Distribution of the Kuiper belt's scattering objects. Astrophys. J. 764, L2–L5.
Sheppard, S.S., 2012. The color differences of Kuiper belt objects in resonance with Neptune. Astron. J. 144, 169–182.
Sicardy, B. et al., 2006. Charon's size and an upper limit on its atmosphere from a stellar occultation. Nature 439, 52–54.
Singer, K.N., McKinnon, W.B., Nowicki, L.T., 2013. Secondary craters from large impacts on Europa and Ganymede: Ejecta size-velocity distributions on icy worlds, and the scaling of ejected blocks. Icarus 226, 865–884.
Solontoi, M. et al., 2012. Ensemble properties of comets in the Sloan Digital Sky Survey. Icarus 218, 571–584.
Stansberry, J. et al., 2008. Physical properties of Kuiper belt and Centaur objects: Constraints from the Spitzer Space Telescope. In: Barucci, M.A., Boehnhardt, H., Cruikshank, D.P., Morbidelli, A. (Eds.), The Solar System Beyond Neptune. University of Arizona Press, pp. 161–179.
Stern, S.A., 2009. Ejecta exchange and satellite color evolution in the Pluto system, with implications for KBOs and asteroids with satellites. Icarus 199, 571–573.
Stern, S.A., Porter, S.A., Zangari, A., 2015. On the roles of escape erosion and the viscous relaxation of craters on Pluto. Icarus 250, 287–293.
Szabó, G.M. et al., 2007. The properties of jovian trojan asteroids listed in SDSS moving object catalogue 3. Mon. Not. R. Astron. Soc. 377, 1393–1406.
Tiscareno, M., Malhotra, R., 2009. Chaotic diffusion of resonant Kuiper belt objects. Astron. J. 138, 827–837.
Trujillo, C.A. et al., 2001. Large bodies in the Kuiper belt. Astron. J. 122, 2740–2748.
Tsiganis, K. et al., 2005. Origin of the orbital architecture of the giant planets of the Solar System. Nature 435, 459–461.
Vokrouhlický, D., Pokorný, P., Nesvorný, D., 2012. Öpik-type collision probability for high-inclination orbits. Icarus 219, 150–160.
Weissman, P.R., Stern, S.A., 1994. The impactor flux in the Pluto–Charon system. Icarus 111, 378–386.
Wetherill, G.W., 1967. Collisions in the asteroid belt. J. Geophys. Res. 72, 2429.
Young, L.A. et al., 2008. New Horizons: Anticipated scientific investigations at the Pluto system. Space Sci. Rev. 140, 93–127.
Zahnle, K., Dones, L., Levison, H., 1998. Cratering rates on the Galilean satellites. Icarus 136, 202–222.
Zahnle, K. et al., 2003. Cratering rates in the outer Solar System. Icarus 163, 263–289.